General Factorization of Conjugate-Symmetric Hadamard Transforms

Seisuke Kyochi, *Member, IEEE*, and Yuichi Tanaka, *Member, IEEE*

***Abstract*—Complex-valued conjugate-symmetric Hadamard transforms ($\mathbb{C}$-CSHT) are variants of complex Hadamard transforms and found applications in signal processing. In addition, their real-valued transform counterparts ($\mathbb{R}$-CSHTs) perform comparably with Hadamard transforms (HTs) despite their lower computational complexity. Closed-form factorizations of $\mathbb{C}$-CSHTs and $\mathbb{R}$-CSHTs have recently been proposed to make calculations more efficient. However, there is still room to find effective and general factorizations. This paper presents a simple closed-form complete factorization of $\mathbb{C}$-CSHTs based on that of $\mathbb{R}$-CSHTs. The proposed factorization can be applied to both $\mathbb{C}$- and $\mathbb{R}$-CSHTs with one factorization and it provides several benefits: 1) It can save total implementation costs for both $\mathbb{C}$-CSHTs and $\mathbb{R}$-CSHTs; 2) the generalized $\mathbb{R}$-CSHT factorization significantly reduces its computational cost; 3) memory-saved local orientation detection of images can be achieved; 4) a fast direction-aware transform can be attained; 5) it clarifies that $\mathbb{C}$- and $\mathbb{R}$-CSHTs are closely related to common block transforms, such as the discrete Fourier transform (DFT), binDCT, and HT; and 6) it achieves a new integer complex-valued transform, which can approximate the DFT better than the original $\mathbb{C}$-CSHT. The image orientation estimation and performance in image coding of our $\mathbb{R}$-CSHTs were evaluated through examples of practical applications based on the proposed factorization.**

***Index Terms*—BinDCT, complex Hadamard transform, conjugate-symmetric sequency-ordered Hadamard transform, DCT, Hadamard transform.**

I. Introduction

HADAMARD transforms (HTs) [1]–[11] have been widely studied for a long time and used for various signal processing and communication applications. Without being exhaustive, they include image compression [2], image watermarking [3], face recognition [4], motion estimation [5], multicarrier CDMA systems [6], and multiband OFDM ultrawideband systems [7]. They have very low computational complexity since each element of their transformation matrices is 1 or -1. The HTs can be classified into several types in terms of orders, i.e., dyadic, natural, and sequency orders [12]. Although the type is chosen according to applications, sequency order is commonly preferred and is often used. This is because sequency is defined as one half the average number of zero crossings per unit time in the unit circle of a complex plane, which is analogous to the frequency of a discrete Fourier transform (DFT).

Until now, various extended versions of HTs have been proposed. They are classified into two categories. The first is the real matrix class such as *antipodal* transforms [13] and lapped HTs [14]. The second is the complex matrix class, which includes unified complex Hadamard transforms (UCHTs) [15] and complex HTs [16]. Complex-valued HTs consist of $\{\pm 1, \pm\sqrt{-1}\}$ and can be recursively generated by the Kronecker product.

Since these complex-valued HTs do not form sequency orders, complex-valued sequency-ordered HTs ($\mathbb{C}$SO-HTs) have been developed [17]. Due to sequency order, the $\mathbb{C}$SO-HTs can behave like DFTs in practical applications. Nevertheless, it has been pointed out that their spectrum is not conjugate-symmetric as it is with DFTs, and thus more memory is needed to store the transformed coefficients.

Complex-valued sequency-ordered conjugate-symmetric HTs ($\mathbb{C}$SO-CSHT), whose spectrum is conjugate-symmetric, have been proposed by permutating complex-valued natural-ordered conjugate-symmetric HTs ($\mathbb{C}$NO-CSHT) to reduce the redundancy of $\mathbb{C}$SO-HTs [18]–[20]. They are more closely related to the frequency of DFTs than that of $\mathbb{C}$SO-HTs and are used in several applications [18], [20]. Moreover, the row vectors of the $\mathbb{C}$SO-CSHT matrix can be regrouped according to conjugate-symmetric properties to obtain corresponding real-valued sinusoidal waves with respective frequencies. These real versions of SO-CSHTs have been denoted $\mathbb{R}$SO-CSHT in this paper. It is worth noting that $\mathbb{R}$SO-CSHTs perform comparably with HTs in a few applications, such as image coding [18], despite their lower computational complexity.

Although they have been well developed in terms of theoretical aspects and practical applications, problems remain in efficiently factorizing them. This paper addresses the factorization problem in complex-valued CSHTs and real-valued CSHTs ($\mathbb{C}$-CSHTs and $\mathbb{R}$-CSHTs) both for natural-ordered and sequency-ordered versions. The factorizations of both $\mathbb{C}$-CSHTs and $\mathbb{R}$-CSHTs in the original paper by Aung *et al.* [18] were only presented for $M = 2^3$, where M is the number of dimensions. Unfortunately, $\mathbb{C}$-CSHT and $\mathbb{R}$-CSHT factorizations were not consistent: One factorization cannot be derived

Manuscript received September 26, 2013; revised March 04, 2014; accepted May 08, 2014. Date of publication May 23, 2014; date of current version June 17, 2014. The associate editor coordinating the review of this manuscript and approving it for publication was Prof. Trac D. Tran. This work was supported by JSPS KAKENHI Grant Number 24860055. Y. Tanaka is supported in part by MEXT Tenure Track Promotion Program. Partial results in this paper has been previously published in the *Proceedings of the International Conference on Acoustics, Speech and Signal Processing* [23].

S. Kyochi is with the Department of Information and Media Engineering, Faculty of Environmental Engineering, The University of Kitakyushu, Kitakyushu, Fukuoka 808-0135, Japan (e-mail: s-kyochi@kitakyu-u.ac.jp).

Y. Tanaka is with Graduate School of Bio-Applications and Systems Engineering (BASE), Tokyo University of Agriculture and Technology, Koganei, Tokyo 184-8588, Japan (e-mail: ytnk@cc.tuat.ac.jp).

Color versions of one or more of the figures in this paper are available online at http://ieeexplore.ieee.org.

Digital Object Identifier 10.1109/TSP.2014.2326620

TABLE I
COMPARISON OF TECHNICAL CONTENTS ON $\mathbb{C}$-CSHTS AND $\mathbb{R}$-CSHTS

	[18]	[19], [20]	[23]	This paper
Size of $\mathbb{C}$-CSHT factorization	8×8	$2^N \times 2^N$	$2^N \times 2^N$	$2^N \times 2^N$
Size of $\mathbb{R}$-CSHT factorization	8×8	——	$2^N \times 2^N$	$2^N \times 2^N$
Consistency of factorization	——	——	✓	✓
Completeness of factorization	——	——	——	✓
Comparison with binDCT and HT	——	——	✓	✓
Comparison with DFT	——	——	——	✓
FD$\mathbb{R}$-CSHT	——	——	——	✓
Modified $\mathbb{C}$-CSHT	——	——	——	✓
Local orientation detection of images	——	——	——	✓
FD$\mathbb{R}$-CSHT-based image coding	——	——	——	✓

simply from another. Additionally, no general factorizations for $M = 2^N$ were presented. $\mathbb{C}$-CSHT factorizations for the general $M = 2^N$ were recently proposed by Bouguezel *et al.* [19] and Wu *et al.* [20]. However, their implementations were restricted to the $\mathbb{C}$-CSHT version and the $\mathbb{R}$-CSHT counterpart could not be trivially derived.

Briefly, these previous methods involved two issues that needed to be resolved:

1) General factorization: The CSHT should be factorized for general $M = 2^N$ and have factorizations for both of $\mathbb{C}$-CSHT and $\mathbb{R}$-CSHT.
2) Consistency of factorization: the $\mathbb{C}$-CSHT and $\mathbb{R}$-CSHT should be factorized based on one approach.[1].

Here, the objective for "consistency of factorization" is to provide a cost saving implementation. If two factorizations are consistent with each other, we do not need full implementations of both transforms. That is, if the $\mathbb{R}$-CSHT is implemented once in our factorization, the $\mathbb{C}$-CSHT can be immediately designed by multiplying some simple matrices. Thus, computational resources for each of them can be directly reused for the other one. In addition, it can be derived that if either $\mathbb{C}$- or $\mathbb{R}$-CSHT factorization satisfies completeness, the other also satisfies it due to consistency of factorization.

This paper presents the most general factorization of CSHTs thus far. First, the $\mathbb{R}$-CSHT factorization of the general 2^N dimensions was newly developed. Based on the generalized $\mathbb{R}$-CSHT factorization, a consistent factorization of $\mathbb{C}$- and $\mathbb{R}$-CSHTs is presented. The proposed consistent factorization indicates theoretical completeness of both $\mathbb{C}$- and $\mathbb{R}$-CSHTs. A comparison of CSHT factorizations is summarized in Table I.

Six main benefits are derived thanks to the consistent factorization.

1) As previously mentioned, it saves implementation costs for both $\mathbb{C}$- and $\mathbb{R}$-CSHTs.
2) The computational cost for any $2^N \times 2^N$ $\mathbb{R}$-CSHTs can be significantly reduced.
3) Since the $\mathbb{R}$-CSHTs, i.e., integer-to-integer transforms, can extract local orientations of images with the same memory size as that of the original image, a memory-saved local orientation estimation of images can be achieved, whereas integer-to-complex transforms, e.g., the conventional $\mathbb{C}$-CSHT and DFT, require a memory size twice that of the original images.
4) Furthermore, fast direction-aware non-redundant image transformation can be achieved from our factorization. This transform is called a *fast directional* $\mathbb{R}$*-CSHT* (FD$\mathbb{R}$-CSHT) in this paper.
5) The structures of the $\mathbb{C}$- and $\mathbb{R}$-CSHTs based on the proposed factorization clarify the structural relationship with other basic transforms, such as the binDCT [21], [22], HT, and DFT.
6) By appending some trivial integer matrices, a new integer complex-valued transform can be attained, which is proposed as a *modified* $\mathbb{C}$*-CSHT*. It can approximate the frequency responses of the DFT better than the original $\mathbb{C}$-CSHT.

The proposed $\mathbb{R}$-CSHT factorization was applied to image orientation analysis and image coding as application examples in the simulation. Our preliminary work [23] demonstrated neither the theoretical completeness of factorization for $\mathbb{C}$- and $\mathbb{R}$-CSHTs, realization of FD$\mathbb{R}$-CSHT and modified $\mathbb{C}$-CSHT, structural factorization comparison between $\mathbb{C}$-CSHT and DFT, memory-saved image orientation analysis, nor image coding performance, as summarized in Table I.

The rest of the paper is organized as follows. Section II reviews the definitions and the conventional factorizations of the $\mathbb{C}$- and $\mathbb{R}$-CSHTs. The proposed closed-form factorization is explained in Section III. The completeness and computational complexity, the method of local orientation detection of the proposed factorization, and FD$\mathbb{R}$-CSHTs are also discussed. Section IV clarifies that our $\mathbb{R}$-CSHT is related to the binDCT and a few other block transforms such as the HT and DFT. Moreover, a modified $\mathbb{C}$-CSHT was derived. Section V provides a numerical evaluation of computational complexity, performance in image orientation estimation, and performance in image coding of the proposed $\mathbb{R}$-CSHTs. Section VI concludes this paper.

Notations

Matrices are indicated in upper-case bold face letters. A matrix with a size of $2^N \times 2^N$ is denoted by subscript $\cdot_N$. The j expresses unit complex number $\sqrt{-1}$. The $2^N \times 2^N$ identity and reverse-identity matrices correspond to $\mathbf{I}_N$ and $\mathbf{J}_N$. The null matrix is $\mathbf{0}$. The i-th row and j-th column entry of matrix $\mathbf{A}$ is described as $\mathbf{A}(i, j)$.

II. PRELIMINARIES

This section first reviews the structures of the $\mathbb{C}$-CSHT and $\mathbb{R}$-CSHT. Then, conventional factorizations are presented.

[1]Consistency of factorization in this paper can be described as follows: let $\mathbf{C}$ be the $\mathbb{C}$-CSHT and $\mathbf{R} = \prod_{k=0}^{N-1} \mathbf{R}_k$ be the $\mathbb{R}$-CSHT factorized by $\{\mathbf{R}_k\}$. Then, $\mathbf{C}$ can be represented as the product of $\mathbf{R}$ with some matrix $\mathbf{X}$ ($\mathbf{C} = \mathbf{XR}$).

Definitions of $\mathbb{C}$NO-*CSHT,* $\mathbb{C}$SO-*CSHT, and* $\mathbb{R}$SO-*CSHT*

We first define the $\mathbb{C}$NO-CSHT based on a recursive expression in this section. Let $\boldsymbol{\mathcal{H}}_N$ be a $2^N \times 2^N$ $\mathbb{C}$NO-CSHT matrix, where $N \geq 1$. Then, this is defined [18] by:

$$\boldsymbol{\mathcal{H}}_N = \begin{bmatrix} \boldsymbol{\mathcal{H}}_{N-1} & \boldsymbol{\mathcal{H}}_{N-1} \\ \widetilde{\boldsymbol{\mathcal{H}}}_{N-1}\mathbf{S}_{N-1} & -\widetilde{\boldsymbol{\mathcal{H}}}_{N-1}\mathbf{S}_{N-1}, \end{bmatrix}, \tag{1}$$

where

$$\mathbf{S}_{N-1} = \begin{bmatrix} \mathbf{I}_{N-2} & \\ & j\mathbf{I}_{N-2} \end{bmatrix},$$
$$\widetilde{\boldsymbol{\mathcal{H}}}_{N-1} = \begin{bmatrix} \widetilde{\boldsymbol{\mathcal{H}}}_{N-2} & \widetilde{\boldsymbol{\mathcal{H}}}_{N-2} \\ \widetilde{\boldsymbol{\mathcal{H}}}_{N-2}\widetilde{\mathbf{I}}_{N-2} & -\widetilde{\boldsymbol{\mathcal{H}}}_{N-2}\widetilde{\mathbf{I}}_{N-2} \end{bmatrix},$$
$$\widetilde{\mathbf{I}}_{N-2} = \begin{bmatrix} \mathbf{I}_{N-3} & \\ & -\mathbf{I}_{N-3} \end{bmatrix}.$$

The smallest matrices $\boldsymbol{\mathcal{H}}_1$, $\widetilde{\boldsymbol{\mathcal{H}}}_1$, and $\widetilde{\mathbf{I}}_1$ are:

$$\boldsymbol{\mathcal{H}}_1 = \widetilde{\boldsymbol{\mathcal{H}}}_1 = \begin{bmatrix} 1 & 1 \\ 1 & -1 \end{bmatrix},\ \mathbf{S}_1 = \begin{bmatrix} 1 & 0 \\ 0 & j \end{bmatrix},\ \widetilde{\mathbf{I}}_1 = \begin{bmatrix} 1 & 0 \\ 0 & -1 \end{bmatrix}.$$

The $\mathbb{C}$SO-CSHT is formulated by permutating the rows of the $\mathbb{C}$NO-CSHT matrix according to the bit-reversal order.

$$\mathbf{H}_N(p,k) = \boldsymbol{\mathcal{H}}_N(b(p),k), \tag{2}$$

where $b(\cdot)$ represents the function that maps the integer to the corresponding bit-reversal order and $\mathbf{H}_N(p,k)$ denotes a (p,k) element of $\mathbf{H}_N$. For example, $\mathbf{H}_3$ is described as:

$$\mathbf{H}_3 = \begin{bmatrix} \mathbf{H}_3(0,k) \\ \mathbf{H}_3(1,k) \\ \mathbf{H}_3(2,k) \\ \mathbf{H}_3(3,k) \\ \mathbf{H}_3(4,k) \\ \mathbf{H}_3(5,k) \\ \mathbf{H}_3(6,k) \\ \mathbf{H}_3(7,k) \end{bmatrix} = \begin{bmatrix} \boldsymbol{\mathcal{H}}_3(0,k) \\ \boldsymbol{\mathcal{H}}_3(4,k) \\ \boldsymbol{\mathcal{H}}_3(2,k) \\ \boldsymbol{\mathcal{H}}_3(6,k) \\ \boldsymbol{\mathcal{H}}_3(1,k) \\ \boldsymbol{\mathcal{H}}_3(5,k) \\ \boldsymbol{\mathcal{H}}_3(3,k) \\ \boldsymbol{\mathcal{H}}_3(7,k) \end{bmatrix}.$$

Furthermore, since the $\mathbb{C}$SO-CSHT is conjugate-symmetric, a real-valued counterpart of the $\mathbb{C}$SO-CSHT, i.e., the $\mathbb{R}$SO-CSHT $\mathbf{R}_N$, can be derived from $\mathbf{H}_N$ as:

$$\mathbf{R}_N = \begin{bmatrix} \mathbf{H}_N(0,k) \\ \frac{1}{2}(\mathcal{J}\{\mathbf{H}_N(1,k) - \mathbf{H}_N(2^N-1,k)\}) \\ \frac{1}{2}(\mathcal{R}\{\mathbf{H}_N(1,k) + \mathbf{H}_N(2^N-1,k)\}) \\ \vdots \\ \frac{1}{2}(\mathcal{J}\{\mathbf{H}_N(2^{N-1}-1,k) - \mathbf{H}_N(2^{N-1}+1,k)\}) \\ \frac{1}{2}(\mathcal{R}\{\mathbf{H}_N(2^{N-1}-1,k) + \mathbf{H}_N(2^{N-1}+1,k)\}) \\ \mathbf{H}_N(2^{N-1},k) \end{bmatrix}, \tag{3}$$

where k is the column index of the matrix and $\mathcal{R}\{\cdot\}$ and $\mathcal{J}\{\cdot\}$ correspond to real and imaginary parts of the number. A real-valued matrix can similarly be generated from the $\mathbb{C}$NO-CSHT by combining the conjugate-symmetric pair, which is denoted as the $\mathbb{R}$NO-CSHT.

A. Closed-Form Factorizations of $\mathbb{C}$-CSHT and $\mathbb{R}$-CSHT by Aung et al. [18]

The factorizations of the $\mathbb{C}$SO-CSHT and $\mathbb{R}$SO-CSHT were separately presented in the original paper by Aung *et al.* [18] and they were implemented for $N = 3$. The $\mathbb{C}$SO-CSHT is factorized as:

$$\mathbf{H}_3 = \mathbf{P}_{H_3} \begin{bmatrix} \mathbf{W}_1 & & & \\ & \mathbf{W}_1 & & \\ & & \mathbf{W}_1 & \\ & & & \mathbf{W}_1 \end{bmatrix} \begin{bmatrix} \mathbf{I}_1 & & & \\ & \mathbf{S}_1 & & \\ & & \mathbf{I}_1 & \\ & & & \widetilde{\mathbf{I}}_1 \end{bmatrix} \times \begin{bmatrix} \mathbf{W}_2 & \\ & \mathbf{W}_2 \end{bmatrix} \begin{bmatrix} \mathbf{I}_2 & \\ & \mathbf{S}_2 \end{bmatrix} \mathbf{W}_3, \tag{4}$$

where

$$\mathbf{P}_{H_3} = \begin{bmatrix} 1 & 0 & 0 & 0 & 0 & 0 & 0 & 0 \\ 0 & 0 & 0 & 0 & 1 & 0 & 0 & 0 \\ 0 & 0 & 1 & 0 & 0 & 0 & 0 & 0 \\ 0 & 0 & 0 & 0 & 0 & 0 & 1 & 0 \\ 0 & 1 & 0 & 0 & 0 & 0 & 0 & 0 \\ 0 & 0 & 0 & 0 & 0 & 1 & 0 & 0 \\ 0 & 0 & 0 & 1 & 0 & 0 & 0 & 0 \\ 0 & 0 & 0 & 0 & 0 & 0 & 0 & 1 \end{bmatrix},$$
$$\mathbf{W}_N = \begin{bmatrix} \mathbf{I}_{N-1} & \mathbf{I}_{N-1} \\ \mathbf{I}_{N-1} & -\mathbf{I}_{N-1} \end{bmatrix},\ \mathbf{W}_1 = \begin{bmatrix} 1 & 1 \\ 1 & -1 \end{bmatrix}.$$

Note that if $\mathbf{P}_{H_3}$ is removed, (4) is the same as the $\mathbb{C}$NO-CSHT factorization.

On the other hand, a factorization of 8×8 $\mathbb{R}$SO-CSHT $\widehat{\mathbf{R}}_3$ is presented in Aung *et al.* [18] as:

$$\widehat{\mathbf{R}}_3 = \begin{bmatrix} \mathbf{W}_1 & & & \\ & \mathbf{J}_1 & & \\ & & \widetilde{\mathbf{I}}_1\mathbf{W}_1 & \\ & & & \mathbf{W}_1 \end{bmatrix} \begin{bmatrix} \mathbf{W}_2 & \\ & \widehat{\mathbf{J}}_2 \end{bmatrix} \mathbf{W}_3, \tag{5}$$

where $\widehat{\mathbf{J}}_2 = \begin{bmatrix} \mathbf{0} & \mathbf{I}_1 \\ \mathbf{I}_1 & \mathbf{0} \end{bmatrix}$. The factorizations of $\mathbf{H}_3$ and $\widehat{\mathbf{R}}_3$ are given in Fig. 1. Unfortunately, the relationships between these two factorizations are not very clear despite the fact that one of them is just a counterpart of the other.

B. Closed-Form Factorization of $\mathbb{C}$-CSHT by Bouguezel et al. [19]

The algorithm used in Aung *et al.*'s original paper [18] is only given for $N = 3$. Bouguezel *et al.* and Wu *et al.* [19], [20] presented the closed-form representation of the $\mathbb{C}$-CSHT for 2^N $\{N \in \mathbb{N}\}$. The $\mathbb{C}$SO-CSHT structure by Bouguezel *et al.* [19] is represented as:

$$\begin{aligned} \mathbf{H}_N = & \left(\prod_{i=1}^{N-2} (\mathbf{I}_{N-i} \otimes \mathbf{W}_1 \otimes \mathbf{I}_{i-1}) \right. \\ & \times \left(\begin{bmatrix} \begin{bmatrix} \mathbf{I}_1 & \mathbf{0} \\ \mathbf{0} & \mathbf{S}_1 \end{bmatrix} & \mathbf{0} \\ \mathbf{0} & \mathbf{I}_i^* \otimes \begin{bmatrix} \mathbf{I}_1 & \mathbf{0} \\ \mathbf{0} & \widetilde{\mathbf{I}}_1 \end{bmatrix} \end{bmatrix} \otimes \mathbf{I}_{i-1} \right) \Bigg) \\ & \times (\mathbf{I}_1 \otimes \mathbf{W}_1 \otimes \mathbf{I}_{N-2}) \left(\begin{bmatrix} \mathbf{I}_1 & \mathbf{0} \\ \mathbf{0} & \mathbf{S}_1 \end{bmatrix} \otimes \mathbf{I}_{N-2} \right) \\ & \times (\mathbf{W}_1 \otimes \mathbf{I}_{N-1}) \end{aligned} \tag{6}$$

where $\otimes$ represents a Kronecker product operator and $\mathbf{I}_i^*$ denotes the identity matrix with the size of $(2^{N-i-1}-1) \times (2^{N-i-1}-1)$. This factorization requires the same number of arithmetic operations as those in the original $\mathbb{C}$SO-CSHT for

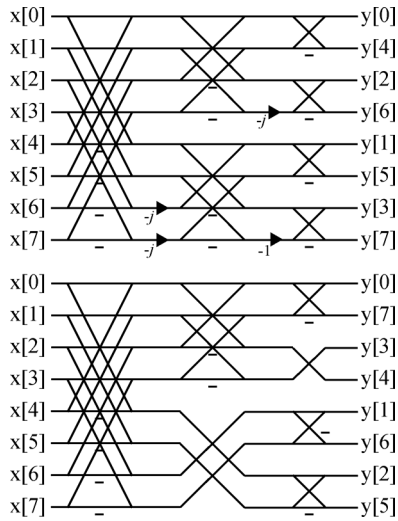

Fig. 1. CSHT factorization in Aung *et al.*'s original paper. Top: $\mathbb{C}$SO-CSHT. Bottom: $\mathbb{R}$SO-CSHT.

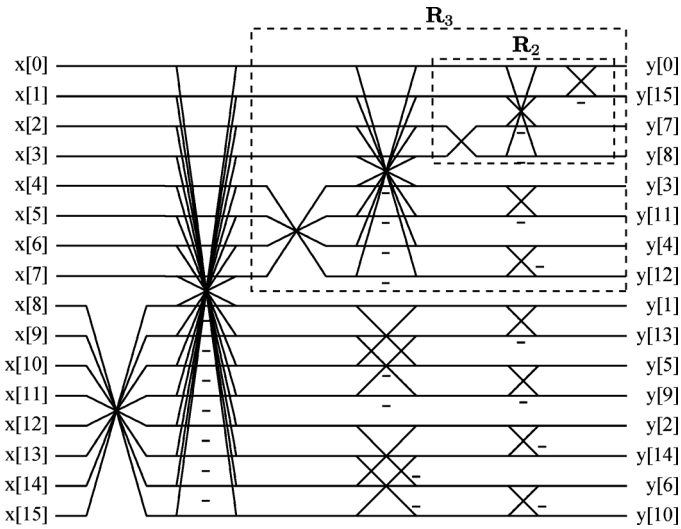

Fig. 2. Sixteen-point $\mathbb{R}$-CSHT based on our factorization where dashed boxes represent four- and eight-point $\mathbb{R}$-CSHTs.

$N = 3$, but provides a more general structure according to N. Wu *et al.* also presented a similar factorization of the $\mathbb{C}$-CSHT [20].

III. Proposed Closed-Form Factorization

This section presents a general closed-form factorization of the $\mathbb{C}$-CSHT. It is expressed as a combination of the $\mathbb{R}$-CSHT and postprocessing with a complex-valued matrix. Similar to Bouguezel *et al.*'s previous factorization [19], let us consider the case for 2^N ($N \in \mathbb{N}$).

A. Generalized Factorization of $\mathbb{R}$-CSHT

We start by generalizing the $\mathbb{R}$-CSHT in (5), which is in contrast to the conventional factorizations. The factorization of $\mathbf{R}_N$ is represented as:

$$\mathbf{R}_N = \begin{bmatrix} \mathbf{R}_{N-1} & \\ & \overline{\mathbf{W}}_{N-1} \end{bmatrix} \overline{\mathbf{I}}_N, \tag{7}$$

where

$$\begin{aligned} \overline{\mathbf{W}}_{N-1} &= \begin{bmatrix} \mathbf{W}^u_{N-2} & \\ & \mathbf{W}^d_{N-2} \end{bmatrix}, \\ \mathbf{W}^u_{N-2} &:= \prod_{k=1}^{N-2} \mathbf{I}_{N-2-k} \otimes \mathbf{W}_k, \\ \mathbf{W}^d_{N-2} &:= \prod_{k=1}^{N-2} \mathbf{I}_{N-2-k} \otimes \widetilde{\mathbf{W}}_k, \\ \widetilde{\mathbf{W}}_N &= \begin{bmatrix} \mathbf{I}_{N-1} & \mathbf{I}_{N-1} \\ -\mathbf{I}_{N-1} & \mathbf{I}_{N-1} \end{bmatrix}, \\ \overline{\mathbf{I}}_N &= \begin{bmatrix} \mathbf{I}_{N-1} & \mathbf{J}_{N-1} \\ \mathbf{J}_{N-1} & -\mathbf{I}_{N-1} \end{bmatrix} \begin{bmatrix} \mathbf{I}_{N-1} & \\ & \mathbf{J}_{N-1} \end{bmatrix}. \end{aligned} \tag{8}$$

Moreover, the 2×2 and 4×4 $\mathbb{R}$-CSHT matrices are defined as:

$$\mathbf{R}_1 = \mathbf{W}_1,\ \mathbf{R}_2 = \begin{bmatrix} \mathbf{W}_1 & \\ & \mathbf{I}_1 \end{bmatrix} \overline{\mathbf{I}}_2\ \left(\overline{\mathbf{W}}_1 = \mathbf{I}_1\right). \tag{9}$$

Note that the proposed $\mathbb{R}$-CSHT is the generalized version of $\widehat{\mathbf{R}}_3$. More specifically, by using the relationship of:

$$\mathbf{W}_N = \begin{bmatrix} \mathbf{I}_{N-1} & \\ & \mathbf{J}_{N-1} \end{bmatrix} \overline{\mathbf{I}}_N,$$

it can be shown that $\mathbf{R}_3$ is equivalent to $\widehat{\mathbf{R}}_3$ as:

$$\begin{aligned} \widehat{\mathbf{R}}_3 &= \begin{bmatrix} \mathbf{W}_1 & & & \\ & \mathbf{I}_1 & & \\ & & \mathbf{W}^u_1 & \\ & & & \mathbf{W}^d_1 \end{bmatrix} \begin{bmatrix} \overline{\mathbf{I}}_2 & \\ & \mathbf{I}_2 \end{bmatrix} \overline{\mathbf{I}}_3 \\ &= \begin{bmatrix} \mathbf{R}_2 & \\ & \overline{\mathbf{W}}_2 \end{bmatrix} \overline{\mathbf{I}}_3 = \mathbf{R}_3. \end{aligned}$$

There is a diagram of the proposed structure for $N = 4$ in Fig. 2. Clearly, our $\mathbb{R}$-CSHT factorization yields a simple recursive implementation. It should be noted that the above discussion is the same as that in our preliminary results without theoretical completeness [23].

B. Completeness of Proposed $\mathbb{R}$-CSHT Factorization and Consistent Factorization for $\mathbb{C}$- and $\mathbb{R}$-CSHTs

This section provides a theoretical discussion concerning the completeness of the proposed $\mathbb{R}$-CSHT. A consistent factorization for both $\mathbb{C}$- and $\mathbb{R}$-CSHTs is also derived.

Reformulate the definition of the $\mathbb{R}$-CSHT (3) as:

$$\mathbf{R}_N = \begin{bmatrix} 1 & & & \\ & \widehat{\mathbf{W}}_2 & & \\ & & \ddots & \\ & & & \widehat{\mathbf{W}}_2 \\ & & & & 1 \end{bmatrix} \mathbf{P}_{\mathbf{H}_N} \mathbf{H}_N \tag{10}$$

in which $\widehat{\mathbf{W}}_2 = \begin{bmatrix} -\frac{j}{2} & \frac{j}{2} \\ \frac{1}{2} & \frac{1}{2} \end{bmatrix}$ and $\mathbf{P}_{\mathbf{H}_N}$ denotes a permutation matrix. Hence, it is enough to show a closed-form (complex) matrix $\widehat{\mathbf{C}}$ satisfying $\mathbf{H}_N = \widehat{\mathbf{C}}\mathbf{R}_N$ to verify the completeness of the proposed $\mathbb{R}$-CSHT factorization. From another viewpoint,

$\mathbf{H}_N = \widehat{\mathbf{C}}\mathbf{R}_N$ indicates that the $\mathbb{C}$- and $\mathbb{R}$-CSHTs can be factorized by a single approach, i.e., it yields consistent factorization.

First, complex matrix $\mathbf{C}_N$ and permutation matrix $\mathbf{P}_N$ are defined as:

$$\begin{aligned}
&\mathbf{C}_N = \begin{bmatrix} \mathbf{C}_{N-1} & \\ & \widetilde{\mathbf{C}}_{N-1} \end{bmatrix}, \widetilde{\mathbf{C}}_{N-1} = \begin{bmatrix} \mathbf{D}_{N-2} & \mathbf{J}_{N-2} \\ \mathbf{D}_{N-2}\mathbf{J}_{N-2} & \mathbf{I}_{N-2} \end{bmatrix}, \\
&\mathbf{D}_N = \mathrm{diag}(j, -j, \ldots, (-1)^{2^N-1} j), \\
&\mathbf{P}_N = \begin{bmatrix} \mathbf{P}_{N-1} & \\ & \widetilde{\mathbf{P}}_{N-1} \end{bmatrix}, \widetilde{\mathbf{P}}_{N-1} = \begin{bmatrix} \widetilde{\mathbf{P}}_{N-2} & \\ & \mathbf{J}_{N-2}\widetilde{\mathbf{P}}_{N-2} \end{bmatrix},
\end{aligned} \tag{11}$$

where $\mathrm{diag}(a_0, \ldots, a_{N-1})$ denotes a diagonal matrix whose diagonal elements are $a_0, \ldots, a_{N-1}$. The smallest matrices $\mathbf{C}_1$, $\widetilde{\mathbf{C}}_1$, $\mathbf{P}_1$, and $\widetilde{\mathbf{P}}_1$ are defined as

$$\mathbf{C}_1 = \mathbf{I}_1, \widetilde{\mathbf{C}}_1 = \begin{bmatrix} j & 1 \\ -j & 1 \end{bmatrix}, \mathbf{P}_1 = \widetilde{\mathbf{P}}_1 = \mathbf{I}_1. \tag{12}$$

By using $\mathbf{C}_N$, $\mathbf{P}_N$, and $\mathbf{R}_N$ in (7), the following theorem can be derived.

Theorem 1: The $\mathbb{C}$NO-CSHT $\boldsymbol{\mathcal{H}}_N$ can be factorized as:

$$\boldsymbol{\mathcal{H}}_N = \mathbf{C}_N\mathbf{P}_N\mathbf{R}_N \ \ (\forall N \in \mathbb{N}). \tag{13}$$

Thus, it can also be factorized as:

$$\mathbf{H}_N = \mathbf{C}'_N\mathbf{P}_N\mathbf{R}_N \ \ (\forall N \in \mathbb{N}), \tag{14}$$

where $\mathbf{C}'_N$ represents the row-wise permutated version of $\mathbf{C}_N$ via the bit-reversal order.

Proof: We can verify the theorem by induction. For $N = 1$, it trivially follows that $\mathbf{C}_1\mathbf{P}_1\mathbf{R}_1 = \mathbf{W}_1 = \boldsymbol{\mathcal{H}}_1$. Next, for $N = 2$, the matrix form of $\boldsymbol{\mathcal{H}}_2$ is:

$$\begin{aligned}
\boldsymbol{\mathcal{H}}_2 &= \begin{bmatrix} 1 & 1 & 1 & 1 \\ 1 & -1 & 1 & -1 \\ 1 & j & -1 & -j \\ 1 & -j & -1 & j \end{bmatrix}, \\
\mathbf{C}_2\mathbf{P}_2\mathbf{R}_2 &= \begin{bmatrix} \mathbf{C}_1 & \\ & \widetilde{\mathbf{C}}_1 \end{bmatrix} \begin{bmatrix} \mathbf{P}_1 & \\ & \widetilde{\mathbf{P}}_1 \end{bmatrix} \begin{bmatrix} \mathbf{W}_1 & \\ & \mathbf{I}_1 \end{bmatrix} \overline{\mathbf{I}}_2 \\
&= \begin{bmatrix} \mathbf{W}_1 & \mathbf{W}_1 \\ \widetilde{\mathbf{C}}_1\mathbf{J}_1 & -\widetilde{\mathbf{C}}_1\mathbf{J}_1 \end{bmatrix}.
\end{aligned}$$

Hence, $\boldsymbol{\mathcal{H}}_2 = \mathbf{C}_2\mathbf{P}_2\mathbf{R}_2$.

Now, let us assume that, for $n \leq N-1$, the following equation is satisfied.

$$\boldsymbol{\mathcal{H}}_n = \mathbf{C}_n\mathbf{P}_n\mathbf{R}_n. \tag{15}$$

Based on this assumption,

$$\boldsymbol{\mathcal{H}}_N = \mathbf{C}_N\mathbf{P}_N\mathbf{R}_N, \tag{16}$$

should be verified. The left-hand side of the assumption in (15) is analyzed as:

$$\boldsymbol{\mathcal{H}}_n = \begin{bmatrix} \boldsymbol{\mathcal{H}}_{n-1} & \\ & \widetilde{\boldsymbol{\mathcal{H}}}_{n-1}\mathbf{S}_{n-1}\mathbf{J}_{n-1} \end{bmatrix} \overline{\mathbf{I}}_N. \tag{17}$$

The right-hand side of (15) is also calculated as:

$$\begin{aligned}
\mathbf{C}_n\mathbf{P}_n\mathbf{R}_n &= \begin{bmatrix} \mathbf{C}_{n-1}\mathbf{P}_{n-1}\mathbf{R}_{n-1} & \\ & \widetilde{\mathbf{C}}_{n-1}\widetilde{\mathbf{P}}_{n-1}\overline{\mathbf{W}}_{n-1} \end{bmatrix} \overline{\mathbf{I}}_N \\
&= \begin{bmatrix} \boldsymbol{\mathcal{H}}_{n-1} & \\ & \widetilde{\mathbf{C}}_{n-1}\widetilde{\mathbf{P}}_{n-1}\overline{\mathbf{W}}_{n-1} \end{bmatrix} \overline{\mathbf{I}}_N,
\end{aligned} \tag{18}$$

where the assumption in (15) is used ($\boldsymbol{\mathcal{H}}_{n-1} = \mathbf{C}_{n-1}\mathbf{P}_{n-1}\mathbf{R}_{n-1}$). Thus, by comparing (17) and (18), the assumption in (15) can be simplified to:

$$\widetilde{\boldsymbol{\mathcal{H}}}_{n-1}\mathbf{S}_{n-1}\mathbf{J}_{n-1} = \widetilde{\mathbf{C}}_{n-1}\widetilde{\mathbf{P}}_{n-1}\overline{\mathbf{W}}_{n-1}, \tag{19}$$

where $n \leq N-1$. Furthermore, from the definition of both sides of the assumption in (19), it can further be calculated as:

$$\begin{aligned}
&\widetilde{\boldsymbol{\mathcal{H}}}_{n-1}\mathbf{S}_{n-1}\mathbf{J}_{n-1} \\
&\quad = \begin{bmatrix} \widetilde{\boldsymbol{\mathcal{H}}}_{n-2} & \widetilde{\boldsymbol{\mathcal{H}}}_{n-2} \\ \widetilde{\boldsymbol{\mathcal{H}}}_{n-2}\widetilde{\mathbf{I}}_{n-2} & -\widetilde{\boldsymbol{\mathcal{H}}}_{n-2}\widetilde{\mathbf{I}}_{n-2} \end{bmatrix} \begin{bmatrix} & \mathbf{J}_{n-2} \\ j\mathbf{J}_{n-2} & \end{bmatrix}, \\
&\widetilde{\mathbf{C}}_{n-1}\widetilde{\mathbf{P}}_{n-1}\widetilde{\mathbf{W}}_{n-1} \\
&\quad = \begin{bmatrix} \mathbf{D}_{n-2} & \mathbf{J}_{n-2} \\ \mathbf{D}_{n-2}\mathbf{J}_{n-2} & \mathbf{I}_{n-2} \end{bmatrix} \\
&\qquad \times \begin{bmatrix} \widetilde{\mathbf{P}}_{n-2}\mathbf{W}^u_{n-2} & \\ & \mathbf{J}_{n-2}\widetilde{\mathbf{P}}_{n-2}\mathbf{W}^d_{n-2} \end{bmatrix}.
\end{aligned} \tag{20}$$

The following condition is finally derived:

$$\begin{aligned}
&\begin{bmatrix} j\widetilde{\boldsymbol{\mathcal{H}}}_{n-2}\mathbf{J}_{n-2} & \widetilde{\boldsymbol{\mathcal{H}}}_{n-2}\mathbf{J}_{n-2} \\ -j\widetilde{\boldsymbol{\mathcal{H}}}_{n-2}\widetilde{\mathbf{I}}_{n-2}\mathbf{J}_{n-2} & \widetilde{\boldsymbol{\mathcal{H}}}_{n-2}\widetilde{\mathbf{I}}_{n-2}\mathbf{J}_{n-2} \end{bmatrix} \\
&\quad = \begin{bmatrix} \mathbf{D}_{n-2}\widetilde{\mathbf{P}}_{n-2}\mathbf{W}^u_{n-2} & \widetilde{\mathbf{P}}_{n-2}\mathbf{W}^d_{n-2} \\ \mathbf{D}_{n-2}\mathbf{J}_{n-2}\widetilde{\mathbf{P}}_{n-2}\mathbf{W}^u_{n-2} & \mathbf{J}_{n-2}\widetilde{\mathbf{P}}_{n-2}\mathbf{W}^d_{n-2} \end{bmatrix}.
\end{aligned} \tag{21}$$

With the same discussion as that for (17) and (18), the problem in (16) can be simplified to:

$$\boldsymbol{\mathcal{H}}_{N-1}\mathbf{S}_{N-1}\mathbf{J}_{N-1} = \widetilde{\mathbf{C}}_{N-1}\widetilde{\mathbf{P}}_{N-1}\overline{\mathbf{W}}_{N-1}. \tag{22}$$

Substituting the definitions in (1), the left-hand side of (22) can be represented as:

$$\begin{aligned}
&\widetilde{\boldsymbol{\mathcal{H}}}_{N-1}\mathbf{S}_{N-1}\mathbf{J}_{N-1} \\
&\quad = \begin{bmatrix} j\widetilde{\boldsymbol{\mathcal{H}}}_{N-2}\mathbf{J}_{N-2} & \widetilde{\boldsymbol{\mathcal{H}}}_{N-2}\mathbf{J}_{N-2} \\ -j\widetilde{\boldsymbol{\mathcal{H}}}_{N-2}\widetilde{\mathbf{I}}_{N-2}\mathbf{J}_{N-2} & \widetilde{\boldsymbol{\mathcal{H}}}_{N-2}\widetilde{\mathbf{I}}_{N-2}\mathbf{J}_{N-2} \end{bmatrix} \\
&\quad = \begin{bmatrix} j\mathbf{X}_{11} & j\mathbf{X}_{11} & \mathbf{X}_{11} & \mathbf{X}_{11} \\ -j\mathbf{X}_{12} & j\mathbf{X}_{12} & -\mathbf{X}_{12} & \mathbf{X}_{12} \\ j\mathbf{X}_{11} & -j\mathbf{X}_{11} & -\mathbf{X}_{11} & \mathbf{X}_{11} \\ -j\mathbf{X}_{12} & -j\mathbf{X}_{12} & \mathbf{X}_{12} & \mathbf{X}_{12}, \end{bmatrix},
\end{aligned} \tag{23}$$

where $\mathbf{X}_{11} = \widetilde{\boldsymbol{\mathcal{H}}}_{N-3}\mathbf{J}_{N-3}$, $\mathbf{X}_{12} = \widetilde{\boldsymbol{\mathcal{H}}}_{N-3}\widetilde{\mathbf{I}}_{N-3}\mathbf{J}_{N-3}$.Then, from the condition in (21), all elements in (23) can be converted to:

$$\begin{aligned}
&\widetilde{\boldsymbol{\mathcal{H}}}_{N-1}\mathbf{S}_{N-1}\mathbf{J}_{N-1} \\
&\quad = \begin{bmatrix} \mathbf{D}_{N-3}\mathbf{X}_{21} & \mathbf{D}_{N-3}\mathbf{X}_{21} & \mathbf{X}_{23} & \mathbf{X}_{23} \\ \mathbf{D}_{N-3}\mathbf{X}_{22} & -\mathbf{D}_{N-3}\mathbf{X}_{22} & -\mathbf{X}_{24} & \mathbf{X}_{24} \\ \mathbf{D}_{N-3}\mathbf{X}_{21} & -\mathbf{D}_{N-3}\mathbf{X}_{21} & -\mathbf{X}_{23} & \mathbf{X}_{23} \\ \mathbf{D}_{N-3}\mathbf{X}_{22} & \mathbf{D}_{N-3}\mathbf{X}_{22} & \mathbf{X}_{24} & \mathbf{X}_{24}, \end{bmatrix},
\end{aligned} \tag{24}$$

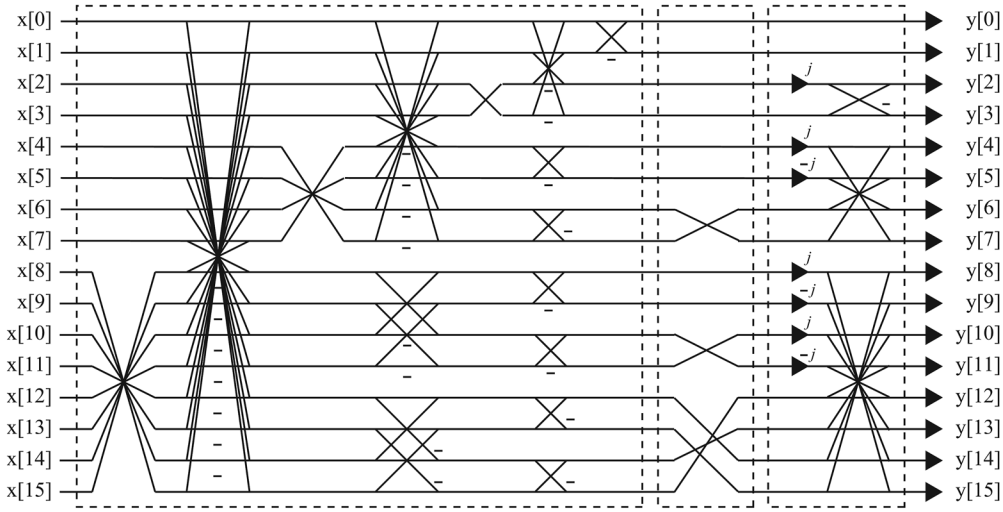

Fig. 3. Sixteen-point $\mathbb{C}$NO-CSHT ($\mathcal{H}_4$) based on our factorization where dashed boxes represent $\mathbf{R}_4$, $\mathbf{P}_4$ and $\mathbf{C}_4$ from left to right.

where $\mathbf{X}_{21} = \widetilde{\mathbf{P}}_{N-3}\mathbf{W}^u_{N-3}$, $\mathbf{X}_{22} = \mathbf{J}_{N-3}\widetilde{\mathbf{P}}_{N-3}\mathbf{W}^u_{N-3}$, $\mathbf{X}_{23} = \widetilde{\mathbf{P}}_{N-3}\mathbf{W}^d_{N-3}$ and $\mathbf{X}_{24} = \mathbf{J}_{N-3}\widetilde{\mathbf{P}}_{N-3}\mathbf{W}^d_{N-3}$. Then, the equation can be calculated as:

$$\begin{aligned}
&\widetilde{\mathcal{H}}_{N-1}\mathbf{S}_{N-1}\mathbf{J}_{N-1}\\
&\quad=\begin{bmatrix}\mathbf{I}_{N-3} & & & \\ & \mathbf{I}_{N-3} & & \\ & & & \mathbf{I}_{N-3}\\ & & \mathbf{I}_{N-3} & \end{bmatrix}\\
&\qquad\times\begin{bmatrix}\mathbf{D}_{N-3}\mathbf{X}_{31} & & \mathbf{X}_{31} & \\ & \mathbf{D}_{N-3}\mathbf{X}_{32} & & \mathbf{X}_{32}\\ \mathbf{D}_{N-3}\mathbf{X}_{32} & & \mathbf{X}_{32} & \\ & \mathbf{D}_{N-3}\mathbf{X}_{31} & & \mathbf{X}_{31}\end{bmatrix}\\
&\qquad\times\begin{bmatrix}\mathbf{W}^u_{N-3} & & & \\ & \mathbf{W}^u_{N-3} & & \\ & & \mathbf{W}^d_{N-3} & \\ & & & \mathbf{W}^d_{N-3}\end{bmatrix}\\
&\qquad\times\begin{bmatrix}\mathbf{W}_{N-2} & \\ & \widetilde{\mathbf{W}}_{N-2}\end{bmatrix}
\end{aligned}$$

where $\mathbf{X}_{31} = \widetilde{\mathbf{P}}_{N-3}$ and $\mathbf{X}_{32} = \mathbf{J}_{N-3}\widetilde{\mathbf{P}}_{N-3}$. Then,

$$\begin{aligned}
&\widetilde{\mathcal{H}}_{N-1}\mathbf{S}_{N-1}\mathbf{J}_{N-1}\\
&=\begin{bmatrix}\mathbf{D}_{N-3}\mathbf{X}_{31} & & \mathbf{X}_{31} & \\ & \mathbf{D}_{N-3}\mathbf{X}_{32} & & \mathbf{X}_{32}\\ & \mathbf{D}_{N-3}\mathbf{X}_{31} & & \mathbf{X}_{31}\\ \mathbf{D}_{N-3}\mathbf{X}_{32} & & \mathbf{X}_{32} & \end{bmatrix}\overline{\mathbf{W}}_{N-1}\\
&=\begin{bmatrix}\mathbf{D}_{N-3} & & & \mathbf{J}_{N-3}\\ & \mathbf{D}_{N-3} & \mathbf{J}_{N-3} & \\ & \mathbf{D}_{N-3}\mathbf{J}_{N-3} & \mathbf{I}_{N-3} & \\ \mathbf{D}_{N-3}\mathbf{J}_{N-3} & & & \mathbf{I}_{N-3}\end{bmatrix}\\
&\quad\times\begin{bmatrix}\widetilde{\mathbf{P}}_{N-3} & & & \\ & \mathbf{J}_{N-3}\widetilde{\mathbf{P}}_{N-3} & & \\ & & & \widetilde{\mathbf{P}}_{N-3}\\ & & \mathbf{J}_{N-3}\widetilde{\mathbf{P}}_{N-3} & \end{bmatrix}\overline{\mathbf{W}}_{N-1}\\
&=\begin{bmatrix}\mathbf{D}_{N-2} & \mathbf{J}_{N-2}\\ \mathbf{D}_{N-2}\mathbf{J}_{N-2} & \mathbf{I}_{N-2}\end{bmatrix}\begin{bmatrix}\widetilde{\mathbf{P}}_{N-2} & \\ & \mathbf{J}_{N-2}\widetilde{\mathbf{P}}_{N-2}\end{bmatrix}\overline{\mathbf{W}}_{N-1}\\
&=\widetilde{\mathbf{C}}_{N-1}\widetilde{\mathbf{P}}_{N-1}\overline{\mathbf{W}}_{N-1}.
\end{aligned}$$

Finally, (22) is satisfied when $n = N$. From the definition of $\mathbb{C}$SO-CSHT, it can be derived that

$$\begin{aligned}
\mathbf{H}_N &= \mathbf{P}^b_N\mathcal{H}_N\\
&= \mathbf{P}^b_N\mathbf{C}_N\mathbf{P}_N\mathbf{R}_N\\
&= \mathbf{C}'_N\mathbf{P}_N\mathbf{R}_N,
\end{aligned}\tag{25}$$

where $\mathbf{P}^b_N$ represents the permutation matrix corresponding to (2). Consequently, $\mathbb{C}$SO-CSHT factorization is obtained by replacing $\mathbf{C}_N$ with $\mathbf{C}'_N$, which is the permutated version of $\mathbf{C}_N$ according to row-wise bit-reversal ordering. ■

Furthermore, $\widetilde{\mathbf{C}}_{N-1}$ ($N \geq 3$) in (11) can be factorized as:

$$\widetilde{\mathbf{C}}_{N-1} = \begin{bmatrix}\mathbf{I}_{N-2} & \mathbf{J}_{N-2}\\ \mathbf{J}_{N-2} & \mathbf{I}_{N-2}\end{bmatrix}\begin{bmatrix}\mathbf{D}_{N-2} & \\ & \mathbf{I}_{N-2}\end{bmatrix}.\tag{26}$$

An example of a 16-channel $\mathbb{C}$NO-CSHT based on (11) and (26) is shown in Fig. 3.

As mentioned in Section II, Aung *et al.* presented factorizations of both $\mathbb{C}$-CSHT and $\mathbb{R}$-CSHT only for $N = 3$ and the factorization of the $\mathbb{R}$-CSHT could not be directly derived from that of the $\mathbb{C}$-CSHT (or vice versa). Moreover, Bouguezel *et al.*'s [19] and Wu *et al.*'s [20] methods are a general $\mathbb{C}$-CSHT factorization in terms of N; however, those of the $\mathbb{R}$-CSHTs were not shown. Our preliminary result of $\mathbb{C}$-CSHT factorization in [23] did not guarantee it was theoretically complete, i.e., the factorization was given heuristically. Furthermore, its permutation matrix had to be determined according to the dimensions. In the above proof of Theorem 1, the complete closed-form factorization of the $\mathbb{C}$-CSHT and $\mathbb{R}$-CSHT is given. Consequently, our factorization provides a consistent, general, and complete form of CSHTs for both real and complex versions.

TABLE II
COMPARISON OF COMPUTATIONAL COMPLEXITIES

	[18]	[19], [20]	Ours
M	8	2^N	2^N
Complex Mul. by j	3	$\frac{M}{2}-1$	$\frac{M}{2}-1$
$\mathbb{C}$-CSHT Add./Sub.	24	$M\log_2 M$	$M\log_2 M$
$\mathbb{R}$-CSHT Add./Sub.	18	N/A	$M(\log_2 M-1)+2$

C. Computational Complexity

The computational complexity of the proposed $\mathbb{C}$-/$\mathbb{R}$-CSHT factorizations is discussed here. The number of complex multiplications by j in the proposed factorization of the $\mathbb{C}$-CSHT is given as follows. From (11) and (26), the number of complex multiplications of $2^N \times 2^N$ $\mathbb{C}$-CSHT can be counted as:

$$\sum_{k=0}^{N-2} 2^k = 2^{N-1} - 1 = \frac{M}{2} - 1. \tag{27}$$

Furthermore, from (11), the number of additions/subtractions in our factorization can be counted as:

$$\underbrace{M(\log_2 M-1)+2}_{\mathbf{R}_N\ (\mathbb{R}-\mathrm{CSHT})} + \underbrace{(M-2)}_{\mathbf{C}_N} = \underbrace{M\log_2 M}_{\boldsymbol{\mathcal{H}}_N\ (\mathbb{C}-\mathrm{CSHT})}. \tag{28}$$

Butterfly matrices for the $\mathbb{R}$-CSHT require $M(\log_2 M-1)+2$ additions/subtractions for $M=2^N$, e.g., 18 additions/subtractions for $N=3$.

Here, the existing factorizations of (4) in Aung *et al.* [18], of (6) in Bouguezel *et al.* [19] and Wu *et al.* [20] are compared. As reported by Aung *et al.* [18] and Bouguezel *et al.* [19], the complex multiplications by j of the $\mathbb{C}$-CSHT ((4) and (6)) are 3 and $\frac{M}{2}-1$, respectively. The complex additions/subtractions are 24 and $M\log_2 M$. Since the factorization by Wu *et al.* [20] is equivalent to that in (6), the complex multiplications and additions/subtractions are the same. Although the sliding algorithm presented by Wu *et al.* [20] can reduce computational complexity in the case of sliding transformation, it is beyond the scope of this paper[2].

Conventional factorization is only presented in Aung *et al.* [18] for the $\mathbb{R}$-CSHT, where there are 18 additions/subtractions. In summary, our general factorization requires the same number of additions/subtractions and complex multiplications for each case as those of the conventional factorizations in specific situations, which is summarized in Table II.

D. Local Orientation Detection and Fast Directional $\mathbb{R}$-CSHT

It is well-known that separable 2-D DFT can analyze directional orientations of images from transformed DFT coefficients. Note that since the DFT is a real-to-complex transformation, memory twice as large as that of the original image is basically required for calculating output coefficients. This subsection explains the use of $\mathbb{C}$-CSHT for local orientation detection, and then describes the method of memory-saved detection based on the proposed factorization, which does not require complex-valued calculations.

[2]In fact, the factorization in Wu et al. [20] is an overcomplete implementation of the $\mathbb{C}$-CSHT.

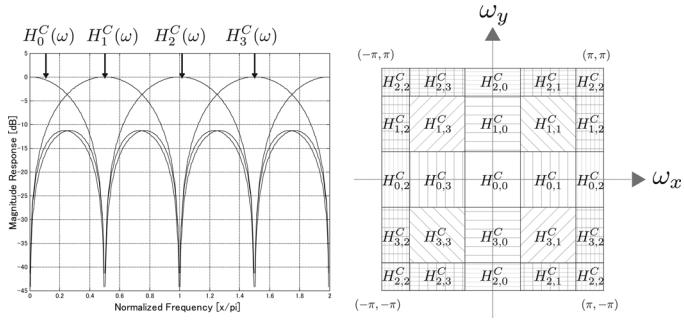

Fig. 4. (Left): Frequency responses $\{H_k^C(\omega)\}_{k=0,\ldots,3}$ of 4×4 $\mathbb{C}$-CSHT ($\mathbf{H}_2$). (Right): 2-D frequency plane partitioning of separable 2-D transform of $\mathbf{H}_2$. $H_{m,n}^C$ ($0\le m,n\le 3$) indicates m-th row and n-th column subband.

For simplicity, we have considered a 4×4 $\mathbb{C}$-CSHT ($\mathbf{H}_2$ in (2)), but it can easily be generalized to any size. Let $H_k^C(\omega)$ ($0\le k\le 3$) be the subband filters corresponding to the k-th row of $\mathbf{H}_2$. Their frequency responses are given in Fig. 4(a). Let $\widetilde{\mathbf{R}}_2$ be the row-wise reordered version of $\mathbf{R}_2$ ((3)) as:

$$\widetilde{\mathbf{R}}_2 = \begin{bmatrix} \mathbf{H}_2(0,k) \\ \frac{1}{2}(\mathcal{R}\{\mathbf{H}_2(1,k)+\mathbf{H}_2(3,k)\}) \\ \mathbf{H}_2(2,k) \\ \frac{1}{2}(\mathcal{J}\{\mathbf{H}_2(1,k)-\mathbf{H}_2(3,k)\}) \end{bmatrix}, \tag{29}$$

and its identical subband filters $H_k^R(\omega)$, $H_k^C(\omega)$ can be represented as:

$$\begin{aligned} H_0^C(\omega) &= H_0^R(\omega), \\ H_1^C(\omega) &= H_1^R(\omega) + jH_3^R(\omega), \\ H_2^C(\omega) &= H_2^R(\omega), \\ H_3^C(\omega) &= H_1^R(\omega) - jH_3^R(\omega). \end{aligned} \tag{30}$$

The separable 2-D $\mathbb{C}$-CSHT decomposes the 2-D frequency plane into subbands as in Fig. 4(b). The amplitude of the subband coefficients implies the strength of each directional component. For example, the transformed coefficients at $H_{1,1}$ exhibit 45 degree directional orientation. 2-D subband filter $H_{1,1}^C(\boldsymbol{\omega})$ ($\boldsymbol{\omega}=(\omega_x,\omega_y)$) corresponding to subband $H_{1,1}$ can be expressed as:

$$\begin{aligned} H_{1,1}^C(\boldsymbol{\omega}) &:= H_1^C(\omega_y)H_1^C(\omega_x) \\ &= (H_1^R(\omega_y)+jH_3^R(\omega_y))(H_1^R(\omega_x)+jH_3^R(\omega_x)) \\ &= (H_1^R(\omega_y)H_1^R(\omega_x) - H_3^R(\omega_y)H_3^R(\omega_x)) \\ &\quad + j(H_1^R(\omega_y)H_3^R(\omega_x) + H_3^R(\omega_y)H_1^R(\omega_x)). \end{aligned} \tag{31}$$

On the other hand, $H_{1,3}^C(\boldsymbol{\omega})$ is

$$\begin{aligned} H_{1,3}^C(\boldsymbol{\omega}) &:= H_1^C(\omega_y)H_3^C(\omega_x) \\ &= (H_1^R(\omega_y)+jH_3^R(\omega_y))(H_1^R(\omega_x)-jH_3^R(\omega_x)) \\ &= (H_1^R(\omega_y)H_1^R(\omega_x) + H_3^R(\omega_y)H_3^R(\omega_x)) \\ &\quad + j(-H_1^R(\omega_y)H_3^R(\omega_x) + H_3^R(\omega_y)H_1^R(\omega_x)). \end{aligned} \tag{32}$$

This indicates that the transformed coefficients corresponding to $H_{1,1}^C(\boldsymbol{\omega})$ can be calculated by those obtained with the 2-D

separable $\mathbb{R}$-CSHT as follows. Let $\mathbf{X}_N$, $\mathbf{Y}_N^C$, and $\mathbf{Y}_N^R$ be a $2^N \times 2^N$ local block of an image and

$$\begin{aligned}\mathbf{Y}_N^C &= \mathbf{H}_N \mathbf{X}_N \mathbf{H}_N^T \\ \mathbf{Y}_N^R &= \widetilde{\mathbf{R}}_N \mathbf{X}_N \widetilde{\mathbf{R}}_N^T,\end{aligned} \tag{33}$$

where $\mathbf{H}_N$ in (2). $\widetilde{\mathbf{R}}_N$ is the row-wise reordered version of $\mathbf{R}_N$ ((3)) as:

$$\widetilde{\mathbf{R}}_N = \begin{bmatrix} \mathbf{H}_N(0,k) \\ \frac{1}{2}(\mathcal{R}\{\mathbf{H}_N(1,k) + \mathbf{H}_N(2^N-1,k)\}) \\ \vdots \\ \frac{1}{2}(\mathcal{R}\{\mathbf{H}_N(2^{N-1}-1,k) + \mathbf{H}_N(2^{N-1}+1,k)\}) \\ \mathbf{H}_N(2^{N-1},k) \\ \frac{1}{2}(\mathcal{J}\{\mathbf{H}_N(2^{N-1}-1,k) - \mathbf{H}_N(2^{N-1}+1,k)\}) \\ \vdots \\ \frac{1}{2}(\mathcal{J}\{\mathbf{H}_N(1,k) - \mathbf{H}_N(2^N-1,k)\}) \end{bmatrix}. \tag{34}$$

The energy of coefficients $|\mathbf{Y}_N^C(m,n)|^2$ can be computed by $\mathbf{Y}_N^R(m,n)$ as:

$$|\mathbf{Y}_N^C(m,n)|^2 = A(m,n)^2 + B(m,n)^2 \tag{35}$$

where

$$\begin{aligned}
&\text{Case 1}: (m,n) \in [1, 2^{N-1}-1] \times [1, 2^{N-1}-1] \\
&\quad \begin{cases} A(m,n) = \mathbf{Y}_N^R(m,n) - \mathbf{Y}_N^R(2^N - m, 2^N - n) \\ B(m,n) = \mathbf{Y}_N^R(m, 2^N - n) + \mathbf{Y}_N^R(2^N - m, n) \end{cases} \\
&\text{Case 2}: (m,n) \in [1, 2^{N-1}-1] \times [2^{N-1}+1, 2^N - 1] \\
&\quad \begin{cases} A(m,n) = \mathbf{Y}_N^R(m, 2^N - n) + \mathbf{Y}_N^R(2^N - m, n) \\ B(m,n) = -\mathbf{Y}_N^R(m,n) + \mathbf{Y}_N^R(2^N - m, 2^N - n) \end{cases} \\
&\text{Case 3}: (m,n) \in [1, 2^{N-1}-1] \times \{0, 2^{N-1}\} \\
&\quad A(m,n) = \mathbf{Y}_N^R(m,n),\ B(m,n) = \mathbf{Y}_N^R(2^N - m, n) \\
&\text{Case 4}: (m,n) \in \{0, 2^{N-1}\} \times [1, 2^{N-1}-1] \\
&\quad A(m,n) = \mathbf{Y}_N^R(m,n),\ B(m,n) = \mathbf{Y}_N^R(m, 2^N - n) \\
&\text{Case 5}: (m,n) \in (0,0),\ (2^{N-1}, 0), \\
&\quad (0, 2^{N-1}),\ (2^{N-1}, 2^{N-1}) \\
&\quad A(m,n) = \mathbf{Y}_N^R(m,n),\ B(m,n) = 0
\end{aligned} \tag{36}$$

Since the complex conjugate relationship implies symmetry ($|\mathbf{Y}_N^C(2^{N-1}+p, 2^{N-1}+q)| = |\mathbf{Y}_N^C(2^{N-1}-p, 2^{N-1}-q)|$), the other coefficients missed in (36) are not required. In this way, local orientation can be detected by using only real-valued (integer) processing. The conventional $\mathbb{C}$-CSHT factorizations [18]–[20] have to convert an image to complex-valued coefficients since the complex calculations in (4) and (6) are inevitable. As a result, the proposed framework can save memory for signal processing.

The above discussion enables us to derive the directional $\mathbb{R}$-CSHT, which is a non-redundant transform and provides directional image representation. Recall that each frequency response of $H_{1,1}^C(\boldsymbol{\omega})$ in (31) or $H_{1,3}^C(\boldsymbol{\omega})$ in (32) only has support in one quadrant of the 2-D frequency plane, as illustrated in Fig. 5(a). By taking the real or imaginary parts of $H_{1,1}^C(\boldsymbol{\omega})$ and $H_{1,3}^C(\boldsymbol{\omega})$, the following relationships can be found:

$$\mathcal{R}[H_{1,1}^C(\boldsymbol{\omega})] = H_1^R(\omega_y)H_1^R(\omega_x) - H_3^R(\omega_y)H_3^R(\omega_x)$$

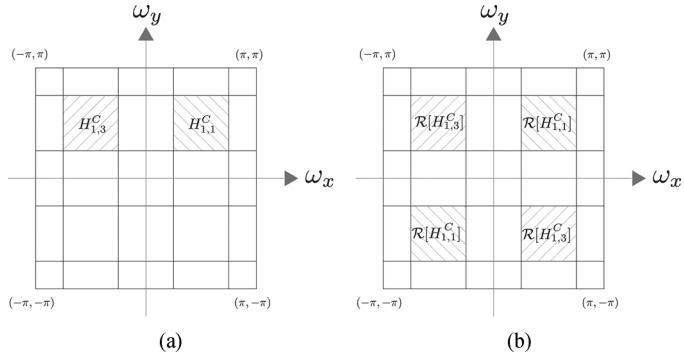

Fig. 5. (a) Frequency responses of $H_{1,1}^C(\boldsymbol{\omega})$ and $H_{1,3}^C(\boldsymbol{\omega})$ corresponding to $H_{1,1}$ and $H_{1,3}$. (b) Frequency responses of real part of $H_{1,1}^C(\boldsymbol{\omega})$ and $H_{1,3}^C(\boldsymbol{\omega})$.

$$\begin{aligned}
\mathcal{J}[H_{1,1}^C(\boldsymbol{\omega})] &= H_1^R(\omega_y)H_3^R(\omega_x) + H_3^R(\omega_y)H_1^R(\omega_x) \\
\mathcal{R}[H_{1,3}^C(\boldsymbol{\omega})] &= H_1^R(\omega_y)H_1^R(\omega_x) + H_3^R(\omega_y)H_3^R(\omega_x) \\
\mathcal{J}[H_{1,3}^C(\boldsymbol{\omega})] &= -H_1^R(\omega_y)H_3^R(\omega_x) + H_3^R(\omega_y)H_1^R(\omega_x).
\end{aligned} \tag{37}$$

As indicated in Fig. 5(b), $\mathcal{R}[H_{1,1}^C(\boldsymbol{\omega})]$ and $\mathcal{R}[H_{1,3}^C(\boldsymbol{\omega})]$ still have the capability of extracting directional components, and $\mathcal{J}[H_{1,1}^C(\boldsymbol{\omega})]$ and $\mathcal{J}[H_{1,3}^C(\boldsymbol{\omega})]$ as well. The output signals of $\mathcal{R}[H_{1,1}^C(\boldsymbol{\omega})]$, $\mathcal{R}[H_{1,3}^C(\boldsymbol{\omega})]$, $\mathcal{J}[H_{1,1}^C(\boldsymbol{\omega})]$, and $\mathcal{J}[H_{1,3}^C(\boldsymbol{\omega})]$ can be derived by using $\mathbb{R}$-CSHT as follows. Let $\mathbf{Y}_N^R(m,n) = \mathbf{R}_N \mathbf{X}_N \mathbf{R}_N^T$, where $\mathbf{R}_N$ is defined in (3). Then, directional output coefficients $\mathbf{Y}_N^d(m,n)$ ($0 \le m,n \le 2^N - 1$) are given as:

$$\begin{aligned}
&\text{Case 1}: (m,n) = (\widetilde{k}, \widetilde{\ell}) \in [1, 2^N - 2] \times [1, 2^N - 2], \\
&\begin{cases} \mathbf{Y}_N^d(\widetilde{k}, \widetilde{\ell}) = c(\mathbf{Y}_N^R(\widetilde{k}, \widetilde{\ell}) - \mathbf{Y}_N^R(\widetilde{k}+1, \widetilde{\ell}+1)) \\ \mathbf{Y}_N^d(\widetilde{k}+1, \widetilde{\ell}+1) = c(\mathbf{Y}_N^R(\widetilde{k}, \widetilde{\ell}) + \mathbf{Y}_N^R(\widetilde{k}+1, \widetilde{\ell}+1)) \\ \mathbf{Y}_N^d(\widetilde{k}+1, \widetilde{\ell}) = c(\mathbf{Y}_N^R(\widetilde{k}, \widetilde{\ell}+1) - \mathbf{Y}_N^R(\widetilde{k}+1, \widetilde{\ell})) \\ \mathbf{Y}_N^d(\widetilde{k}, \widetilde{\ell}+1) = c(\mathbf{Y}_N^R(\widetilde{k}, \widetilde{\ell}+1) + \mathbf{Y}_N^R(\widetilde{k}+1, \widetilde{\ell})) \end{cases}, \\
&\text{Case 2}: \\
&(m,n) \in [0, 2^N - 1] \times [0, 2^N - 1] \backslash [1, 2^N - 2] \times [1, 2^N - 2], \\
&\mathbf{Y}_N^d(m,n) = \mathbf{Y}_N^R(m,n),
\end{aligned} \tag{38}$$

where $\widetilde{k} = 2k+1$ and $\widetilde{\ell} = 2\ell + 1$. If normalization is required, $c = \frac{1}{\sqrt{2}}$, otherwise $c = 1$. Obviously, this process is invertible. The $\mathbb{R}$-CSHT followed by the operation of (38) is denoted as the FD$\mathbb{R}$-CSHT. The number of extra additions/subtractions required for FD$\mathbb{R}$-CSHT is $4(2^{N-1}-1)^2$ and that of the scaling factors is also $4(2^{N-1}-1)^2$. The FD$\mathbb{R}$-CSHT can efficiently work in direction-aware image coding, as will be shown in Section V-B.

IV. Structural Comparison With Basic Transforms

A. Comparison With BinDCT and HT

First, we compare the structure of the $\mathbb{R}$-CSHT with those of the binDCT [21], [22], [25], and HT [1]. All of them are simple transforms whose elements are 1, -1 or 0.

The binDCT is known to be computationally effective form of DCT. It approximates the DCT's transformation matrix with the lifting implementation [24]. It was originally based on Chen *et al.*'s [25] and Loeffler *et al.*'s factorizations [26]. We consider the former in this section. It is implemented with butterfly

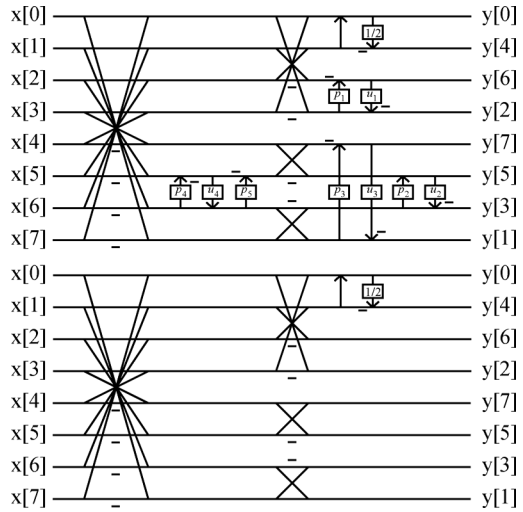

Fig. 6. Structures of binDCT where p_n and u_n are parameters for lifting steps (scaling parameters have been omitted for simplicity). Top: General binDCT structure based on Chen's factorization. Bottom: BinDCT-C9.

matrices and several lifting steps and gives a multiplierless representation of the DCT. Based on the tradeoff between complexity and performance, the binDCT has many configurations. Here, we have focused on the simplest version of the binDCT, which is Liang and Tran's binDCT-C9 [21]. The factorizations of the general binDCT and the binDCT-C9 (8×8) are outlined in Fig. 6.

Liang and Tran [21], compared the structures of the binDCT and HT. Based on binDCT factorization, we can obtain the HT from the binDCT-C9 by appending two butterfly matrices and a trivial $\mathbf{J}_1$ shown in Fig. 7(b). It is clear, on the other hand, that the binDCT-C9 has quite a close structure to that of the $\mathbb{R}$-CSHT (Fig. 7(c)). In fact, the $\mathbb{R}$-CSHT is the same as the binDCT-C9 except for the permutation matrices. The computational complexities of the binDCT-C9 and $\mathbb{R}$-CSHT are the same since the upper right lifting matrix of the binDCT-C9 in Fig. 6 can be represented as one butterfly matrix $\mathbf{W}_2$ in Fig. 7(a) (except for the scaling factor) [21]. Consequently, it can be clarified that the $\mathbb{R}$-CSHT can be regarded as a variant of the binDCT-C9 as well as HT via our factorization.

B. Comparison With DFT and Realization of Modified $\mathbb{C}$-CSHT

Furthermore, we analyzed the important structural relationship between the $\mathbb{C}$-/$\mathbb{R}$-CSHT and DFT. Since the properties of the $\mathbb{C}$-CSHT are analogous to those of the DFT, the $\mathbb{C}$-/$\mathbb{R}$-CSHTs can be expected to have similar factorizations to the DFT.

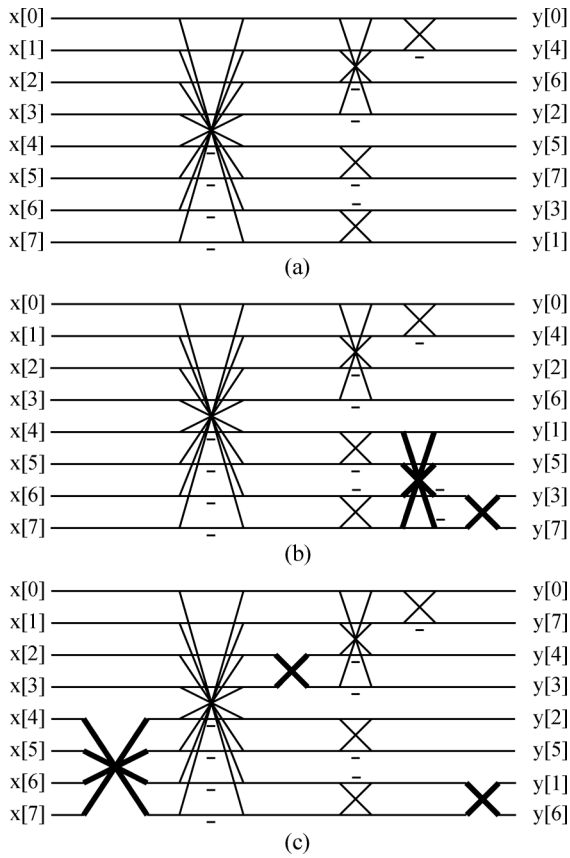

Fig. 7. Comparison of integer-valued transforms. (a) binDCT-C9. (b) HT. (c) $\mathbb{R}$-CSHT. Differences from binDCT-C9 are indicated in bold.

Let $\mathbf{F}_N$ be the DFT matrix defined as $\mathbf{F}_N(k,n) = \exp[-j\frac{2\pi kn}{2^N}]$. Then, it is verified that $\mathbf{F}_N$ ($N \leq 4$) can be factorized as[3]:

$$\begin{aligned}\mathbf{F}_N &= \mathbf{P}_N^{(\mathbf{F})}\mathbf{C}_N\mathbf{P}_N\mathbf{T}_N,\\ \mathbf{T}_N &= \begin{bmatrix}\mathbf{T}_{N-1} & \\ & \overline{\mathbf{W}}_{N-1}\mathbf{\Lambda}_{N-1}\end{bmatrix}\bar{\mathbf{I}}_N,\end{aligned} \tag{39}$$

where $\overline{\mathbf{W}}_{N-1}$, $\mathbf{C}_N$, and $\mathbf{P}_N$ are given in (11), and $\bar{\mathbf{I}}_N$ is in (8). $\mathbf{P}_N^{(\mathbf{F})}$ is a row-wise permutation matrix. $\mathbf{\Lambda}_N$ can be determined by the products of some simple matrices, e.g., butterfly matrices, permutation matrices, and rotation matrices. For example,

$$\mathbf{\Lambda}_1 = \mathbf{I}_1,\ \mathbf{\Lambda}_2 = \begin{bmatrix}\frac{1}{\sqrt{2}} & 0 & \frac{1}{\sqrt{2}} & 0\\ 0 & 1 & 0 & 0\\ -\frac{1}{\sqrt{2}} & 0 & \frac{1}{\sqrt{2}} & 0\\ 0 & 0 & 0 & 1\end{bmatrix}. \tag{40}$$

Fig. 8(a) shows the factorization of $\mathbf{F}_4$. In the figure, $\mathbf{\Lambda}_3 = \mathbf{\Lambda}_{3,3}\mathbf{\Lambda}_{3,2}\mathbf{\Lambda}_{3,1}$, where

[3]A theoretical complete closed-form factorization of (39) for $N > 4$ is one of our future works.

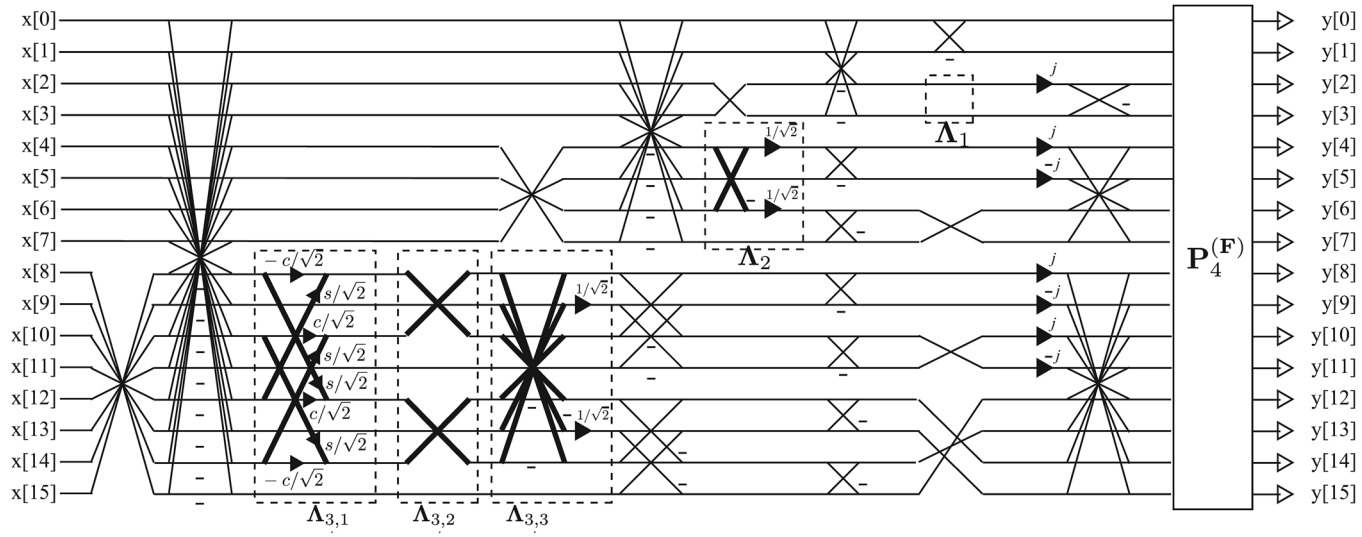

(a)

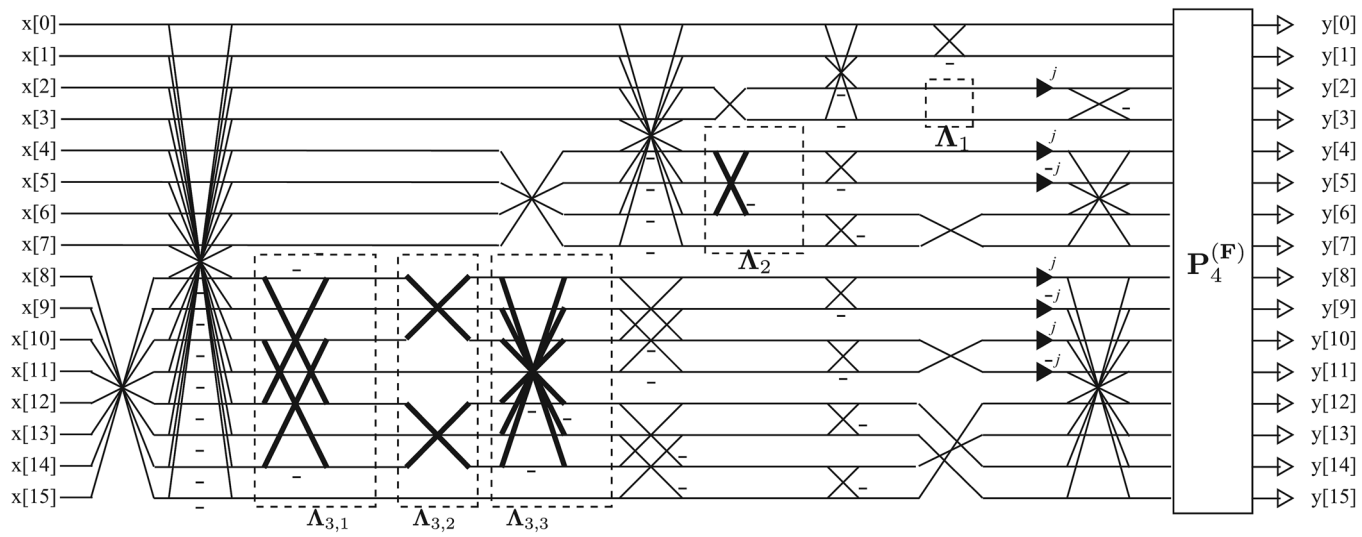

(b)

Fig. 8. (a) Structure of 16×16 DFT factorization related to proposed $\mathbb{C}$-CSHT, where $c = \cos(\frac{3\pi}{8})$ and $s = \sin(\frac{3\pi}{8})$. (b) 16×16 modified $\mathbb{C}$-CSHT derived from (a) by replacing angle $\frac{3\pi}{8}$ with $\frac{\pi}{4}$ and removing multiplications.

$$\mathbf{\Lambda}_{3,1} = \begin{bmatrix} \frac{-c\frac{3\pi}{8}}{\sqrt{2}} & 0 & 0 & 0 & \frac{s\frac{3\pi}{8}}{\sqrt{2}} & 0 & 0 & 0 \\ 0 & 1 & 0 & 0 & 0 & 0 & 0 & 0 \\ 0 & 0 & \frac{c\frac{3\pi}{8}}{\sqrt{2}} & 0 & 0 & 0 & \frac{s\frac{3\pi}{8}}{\sqrt{2}} & 0 \\ 0 & 0 & 0 & 1 & 0 & 0 & 0 & 0 \\ \frac{s\frac{3\pi}{8}}{\sqrt{2}} & 0 & 0 & 0 & \frac{c\frac{3\pi}{8}}{\sqrt{2}} & 0 & 0 & 0 \\ 0 & 0 & 0 & 0 & 0 & 1 & 0 & 0 \\ 0 & 0 & \frac{s\frac{3\pi}{8}}{\sqrt{2}} & 0 & 0 & 0 & \frac{-c\frac{3\pi}{8}}{\sqrt{2}} & 0 \\ 0 & 0 & 0 & 0 & 0 & 0 & 0 & 1 \end{bmatrix},$$

$$\mathbf{\Lambda}_{3,2} = \begin{bmatrix} 0 & 0 & 1 & 0 & 0 & 0 & 0 & 0 \\ 0 & 1 & 0 & 0 & 0 & 0 & 0 & 0 \\ 1 & 0 & 0 & 0 & 0 & 0 & 0 & 0 \\ 0 & 0 & 0 & 1 & 0 & 0 & 0 & 0 \\ 0 & 0 & 0 & 0 & 0 & 0 & 1 & 0 \\ 0 & 0 & 0 & 0 & 0 & 1 & 0 & 0 \\ 0 & 0 & 0 & 0 & 1 & 0 & 0 & 0 \\ 0 & 0 & 0 & 0 & 0 & 0 & 0 & 1 \end{bmatrix},$$

$$\mathbf{\Lambda}_{3,3} = \begin{bmatrix} 1 & 0 & 0 & 0 & 0 & 0 & 1 & 0 \\ 0 & \frac{1}{\sqrt{2}} & 0 & 0 & 0 & \frac{1}{\sqrt{2}} & 0 & 0 \\ 0 & 0 & 1 & 0 & 1 & 0 & 0 & 0 \\ 0 & 0 & 0 & 1 & 0 & 0 & 0 & 0 \\ 0 & 0 & 1 & 0 & -1 & 0 & 0 & 0 \\ 0 & -\frac{1}{\sqrt{2}} & 0 & 0 & 0 & \frac{1}{\sqrt{2}} & 0 & 0 \\ 1 & 0 & 0 & 0 & 0 & 0 & -1 & 0 \\ 0 & 0 & 0 & 0 & 0 & 0 & 0 & 1 \end{bmatrix}, \quad (41)$$

where $c_{\frac{3\pi}{8}} = \cos(\frac{3\pi}{8})$ and $s_{\frac{3\pi}{8}} = \sin(\frac{3\pi}{8})$. By comparing Fig. 3 with Fig. 8(a), $\mathbf{F}_N$ is very similar to the $\mathbb{C}$-CSHT except for some trivial matrices. Thus, the proposed $\mathbb{C}$-/$\mathbb{R}$-CSHT factorization has a very close relationship with that of the DFT.

Interestingly, a new integer complex-valued approximation of the DFT, which is denoted as a *modified* $\mathbb{C}$-*CSHT*, can be proposed inspired by the factorization of $\mathbf{F}_N$ in (39). We can construct an integer-valued approximated transform in the same way of [22], by replacing the real matrices in the DFT factor-

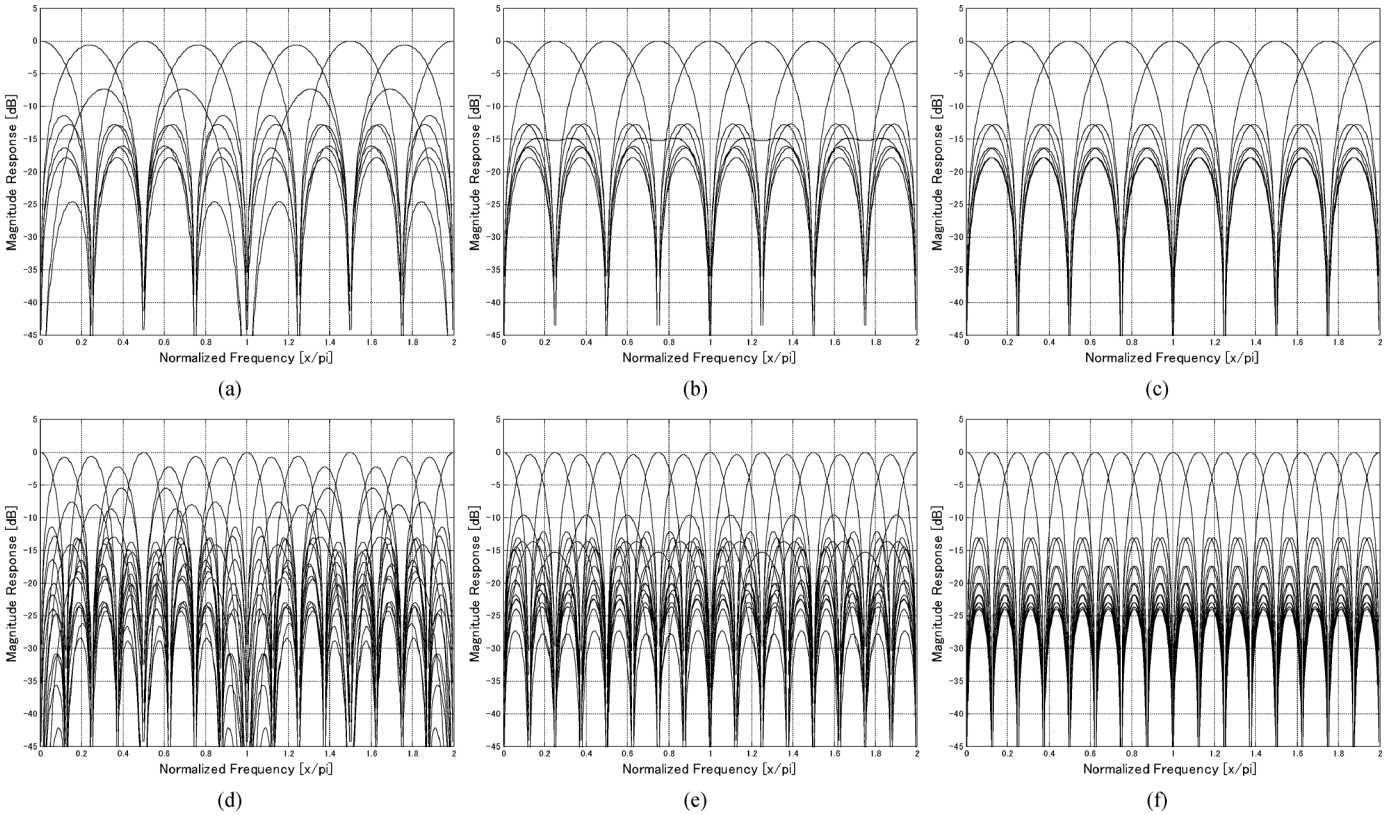

Fig. 9. Frequency responses of $\mathbb{C}$-CSHT (left), modified $\mathbb{C}$-CSHT (middle), and DFT (right). (a), (b), and (c): 8×8, and (d), (e), and (f): 16×16. (a) $\mathbb{C}$-CSHT. (b) Modified $\mathbb{C}$-CSHT. (c) DFT. (d) $\mathbb{C}$-CSHT. (e) Modified $\mathbb{C}$-CSHT. (f) DFT.

TABLE III
NUMBER OF REAL/COMPLEX ADDITIONS AND MULTIPLICATIONS

	$\mathbb{C}$-CSHT			modified $\mathbb{C}$-CSHT			DFT		
Matrix size	4×4	8×8	16×16	4×4	8×8	16×16	4×4	8×8	16×16
# of additions/subtractions	8	24	64	8	26	76	8	26	76
# of multiplications	1	3	7	1	3	7	1	5	19

ization to integer ones. All the rotation angles in the design of the modified $\mathbb{C}$-CSHT are first set to trivial ones, say 0 or $\frac{\pi}{4}$, and then all the scaling factors are removed. Fig. 8(b) has an example of the 16×16 modified $\mathbb{C}$-CSHT.

Table III summarizes the computational costs of the $\mathbb{C}$-CSHT, modified $\mathbb{C}$-CSHT, and DFT. Their frequency responses are also shown in Fig. 9. Clearly, the modified $\mathbb{C}$-CSHT approximates the frequency responses of the DFT better than the $\mathbb{C}$-CSHT, despite a few extra additions/subtractions and permutation operators.

V. SIMULATION

A. Local Orientation Estimation

One of the main contributions of this paper is that the proposed factorization can reduce the computational cost for arbitrary $2^N \times 2^N$ $\mathbb{R}$-CSHT, whereas the conventional methods can only be applied to 8×8. Moreover, the $\mathbb{R}$-CSHT has the capability for local orientation analysis without having to use complex-valued processing. This subsection evaluates the local orientation estimation of images, as an application of the large $\mathbb{R}$-CSHTs.

As illustrated in Fig. 10, the separable 2-D transform by using $\mathbb{R}$-CSHT $\widetilde{\mathbf{R}}_N$ ((34)) is first applied to each $2^N \times 2^N$ image block $\mathbf{X}_N$ as $\mathbf{Y}_N^R = \widetilde{\mathbf{R}}_N \mathbf{X}_N \widetilde{\mathbf{R}}_N^T$. We used *Zoneplate* (Fig. 10) as a test image, since it contains various directional components. Then, the transformed coefficients $\mathbf{Y}_N^R(m,n)$ are converted to $|\mathbf{Y}_N^C(m,n)|^2$ by using (35) to analyze directional information. The direction index to obtain the maximum amplitude of $|\mathbf{Y}_N^C(m,n)|^2$ can be calculated as:

$$(m^*, n^*) = \arg \max_{(m,n) \in \Omega(N)} |\mathbf{Y}_N^C(m,n)|^2,$$
$$\Omega(N) = [0, N/2] \times [0, N/2] \cup [1, N/2-1] \times [N/2+1, N] \backslash \{(0,0)\}. \quad (42)$$

Finally, the local orientation is determined from (m^*, n^*). For comparison, we use the DFT-based image orientation estimation. For each $2^N \times 2^N$ block, the separable 2-D DFT of $\mathbf{F}_N$ is applied, and the maximum amplitude of the DFT coefficients is found as in (42). The detected results from the DFT are set as the correct direction, and then we count the number of mismatched

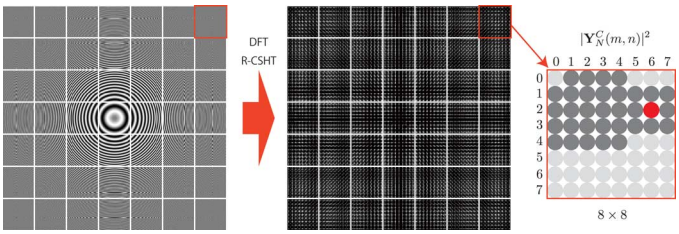

Fig. 10. Overview of local orientation detection (8 × 8). (Left): Original image of *Zoneplate*. (Middle): Amplitude $|\mathbf{Y}_N^C(m,n)|^2$ obtained by $\mathbb{R}$-CSHT or DFT. (Right) Determination of local direction. For example, red coefficient indicates detected one with maximum amplitude.

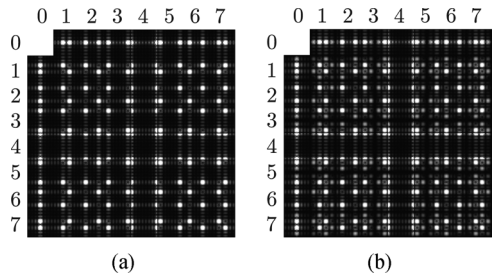

Fig. 11. Amplitude of transformed coefficients rearranged according to same subband. (a): DFT and (b): $\mathbb{R}$-CSHT with postprocessing in (35). (a) DFT. (b) $\mathbb{R}$-CSHT.

TABLE IV
NUMBER OF MISMATCHED BLOCKS

Dim. of $\mathbb{R}$-CSHT and DFT	8 × 8	16 × 16	32 × 32
Number of total blocks	4096	1024	256
Number of mismatched blocks	117	2	0

blocks indicating the different indices between the $\mathbb{R}$-CSHT and DFT.

Fig. 11(a) and (b) show the magnitudes of the transformed coefficients of the DFT and $\mathbb{R}$-CSHT by rearranging the coefficients according to the same subband index. Clearly, the transformed coefficients obtained from the $\mathbb{R}$-CSHT can exhibit the directional components of the test image, as well as those of the DFT. As indicated in Table IV, only 3% of blocks failed for the 8 × 8 case. Moreover, for block sizes of 16 × 16 and 32 × 32, the detected subband indices obtained with the $\mathbb{R}$-CSHT are almost or perfectly matched with those obtained with the DFT. Note that the DFT is complex-valued transform, it basically requires a memory size twice that of the original images. Consequently, the $\mathbb{R}$-CSHTs with large blocks can achieve comparable performance in orientation analysis with the DFT while saving computational cost and memory.

B. Image Coding Example

We evaluated performance in image coding and the practical computational complexities of the $\mathbb{R}$-CSHT as applications of the proposed factorization, which are discussed in this subsection. Aung et. al. also demonstrated similar image coding simulations [21]. However, they only used 8 × 8 dimension in their simulations. Since the proposed factorization provides any dimensions of 2^N, we can obtain results in the case of $N > 3$. We compared four integer transforms, i.e., the HT, binDCT, $\mathbb{R}$-CSHT, and FD$\mathbb{R}$-CSHT. To the best of our knowledge, the

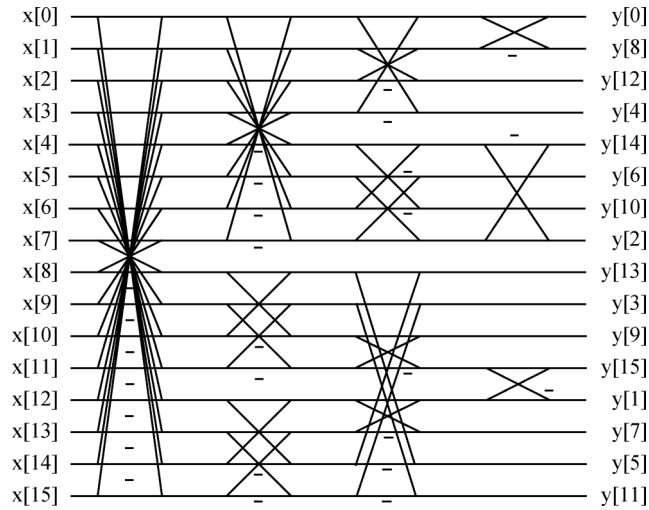

Fig. 12. The 16 × 16 binDCT derived from multiplierless DCT presented in [21] by setting lifting coefficients to zero.

TABLE V
CODING GAIN AND PRACTICAL COMPUTATIONAL COMPLEXITY FOR VARIOUS TRANSFORMS

Coding gain [dB]			
2^N	HT	$\mathbb{R}$-CSHT	binDCT
16	8.194	7.996	7.033
32	8.269	8.175	N/A
64	8.295	8.264	N/A

The number of additions/subtractions per block				
$2^N \times 2^N$	HT	binDCT	$\mathbb{R}$-CSHT	FD$\mathbb{R}$-CSHT
16 × 16	2048	1632	1600	1796
32 × 32	10240	N/A	8320	9220
64 × 64	49152	N/A	41216	45060

The number of multiplications per block				
$2^N \times 2^N$	HT	binDCT	$\mathbb{R}$-CSHT	FD$\mathbb{R}$-CSHT
16 × 16	512	512	512	512
32 × 32	2048	N/A	2048	2048
64 × 64	8192	N/A	8192	8192

16-point binDCT corresponding to the binDCT-C9 has not been officially presented. One possible realization is only simplifying Loeffler *et al.*'s 16-point binDCT factorization [21] in the same way as the binDCT-C9, i.e., removing all the lifting steps. The binDCT obtained from the multiplierless DCT by setting lifting coefficients to zero is illustrated in Fig. 12. Each transform matrix, which is denoted as $\mathbf{A}_N$, is normalized to be orthogonal by multiplying scaling matrix $\mathbf{\Gamma}_N$ as $\mathbf{\Gamma}_N\mathbf{A}_N$.

Table V compares the coding gain and practical implementation cost, i.e., the numbers of additions/subtractions and multiplications per block. The proposed $\mathbb{R}$-CSHT requires less computational cost than the HT and binDCT, and achieves higher coding gain than the binDCT. Note that the conventional 16 × 16 $\mathbb{R}$-CSHT in [18] requires higher computational cost, which is equal to 4096 additions/subtractions per block, because no explicit factorization is given. Since larger HT and $\mathbb{R}$-CSHT can easily be derived, additional results are listed in Table V. It indicates the coding gains of both transforms are saturated as the transforms increase in size and they asymptotically approach each other. The computational costs for the

(a) (b)

Fig. 13. Test images: (a) *Lena* and (b) *Barbara*.

TABLE VI
IMAGE CODING RESULTS FOR VARIOUS TRANSFORMS

Barbara				
bpp	HT	binDCT	$\mathbb{R}$-CSHT	FD$\mathbb{R}$-CSHT
0.25	25.73	24.19	25.26	25.69
0.50	27.99	26.41	27.59	27.99
1.00	31.91	29.88	31.55	31.88
1.50	35.28	33.16	34.89	35.19
2.00	38.05	35.63	37.61	37.94
Lena				
bpp	HT	binDCT	$\mathbb{R}$-CSHT	FD$\mathbb{R}$-CSHT
0.25	29.09	27.08	28.60	28.75
0.50	32.05	29.55	31.60	31.80
1.00	35.79	33.14	35.42	35.58
1.50	38.64	36.11	38.15	38.31
2.00	40.72	38.90	40.52	40.60
Zoneplate				
bpp	HT	binDCT	$\mathbb{R}$-CSHT	FD$\mathbb{R}$-CSHT
0.25	11.93	11.30	11.44	12.38
0.50	14.34	13.57	13.87	15.05
1.00	18.24	17.06	17.51	18.89
1.50	21.82	20.25	20.72	22.24
2.00	24.67	22.98	23.52	25.34

$\mathbb{R}$-CSHT, on the other hand, are much lower than those for the HT. Furthermore, the number of additions/subtractions of the FD$\mathbb{R}$-CSHTs are even lower than that of the HTs, despite the additional operations in (38). Note that no additional multiplication is required for the FD$\mathbb{R}$-CSHTs, since the normalization factors c in (38) can be merged with $\mathbf{\Gamma}_N$.

The set partitioning in hierarchical trees (SPIHT) progressive image coding algorithm [27] was used for encoding transformed coefficients. We used three popular test images of *Lena*, *Barbara* (Fig. 13(a) and (b)), and *Zoneplate*. Table VI summarizes the reconstruction error (PSNR [dB]) of several bit rates. It can be seen that the FD$\mathbb{R}$-CSHT improves the image coding performance of the $\mathbb{R}$-CSHT. Moreover, it is highly comparable to the HT. In particular, it consistently outperforms the HT in all bit rates for *Zoneplate*, due to the ability of compact representation for directional components.

VI. CONCLUSION

We presented a general and unified factorization of the $\mathbb{C}$-CSHT and $\mathbb{R}$-CSHT. We first generalized the conventional factorization of the $\mathbb{R}$-CSHT, and then factorized the $\mathbb{C}$-CSHT based on the $\mathbb{R}$-CSHT. Hence, the structure covered both real and complex versions of the CSHT and any dimensions of $M = 2^N$. In addition, we verified that the proposed factorization was complete and the computational complexity of the proposed factorization was the same as that of the conventional one.

The proposed factorization has several useful and important benefits. 1) Its consistency saved the total implementation costs of the $\mathbb{C}$- and $\mathbb{R}$-CSHTs, whereas the conventional factorization needs complete implementations both for the $\mathbb{C}$- and $\mathbb{R}$-CSHTs. 2) While the conventional method could not factorize the $\mathbb{R}$-CSHT for arbitrary 2^N ($N > 3$), the proposed $\mathbb{R}$-CSHT could be applied to arbitrary 2^N and thus significantly reduced the computational cost. 3) Since the proposed factorization is real-valued processing ($\mathbb{R}$-CSHT) followed by complex-valued processing, local image orientations could be analyzed from only real-valued (integer) coefficients obtained from the $\mathbb{R}$-CSHT. Since the conventional factorizations were real-to-complex transforms, they consumed twice as much memory as the original image size. 4) Fast direction-aware non-redundant image transformation, i.e., FD$\mathbb{R}$-CSHT, could be achieved. 5) The proposed factorization clarified that the $\mathbb{R}$-CSHT is very closely related to the binDCT and HT, and the $\mathbb{C}$-CSHT is an integer-valued counterpart of the DFT. 6) Furthermore, by appending some trivial integer matrices to $\mathbb{C}$-CSHT factorization, a modified $\mathbb{C}$-CSHT could be achieved, which approximated the DFT better than the conventional $\mathbb{C}$-CSHT.

The $\mathbb{R}$-CSHT was applied to image orientation estimation and image coding as possible applications. The $\mathbb{R}$-CSHT achieved comparable performance with the DFT in image orientation estimation despite its integer-based processing. On the other hand, the FD$\mathbb{R}$-CSHT presented comparable or superior performances to the HT and the binDCT in image coding, especially for images containing many directional components. We also validated that the coding gains of the $\mathbb{R}$-CSHT and HT were comparable for large blocks.

REFERENCES

[1] K. J. Horadam, *Hadamard Matrices and Their Applications*. Princeton, NJ, USA: Princeton Univ. Press, 2007.

[2] I. Valova and Y. Kosugi, "Hadamard-based image decomposition and compression," *IEEE Trans. Inf. Technol. Biomed.*, vol. 4, pp. 306–319, 2000.

[3] F. Fonda and S. Pastore, "Innovative image watermarking technique for image authentication in surveillance applications," in *Proc. IEEE Int. Workshop Imag. Syst. Techn.*, 2005, pp. 32–35.

[4] M. Faundez-Zanuy, J. Roure, V. Espinosa-Duro, and J. A. Ortega, "An efficient face verification method in a transformed domain," *Pattern Recognit. Lett.*, vol. 28, no. 7, pp. 854–858, 2007.

[5] C. M. Mak, C. K. Fong, and W. K. Cham, "Fast motion estimation for H.264/AVC in Walsh-Hadamard domain," *IEEE Trans. Circuits Syst. Video Technol.*, vol. 18, no. 6, pp. 735–745, 2008.

[6] S. H. Tsai, Y. P. Lin, and C. C. J. Kuo, "MAI-free MC-CDMA systems based on Hadamard-Walsh codes," *IEEE Trans. Signal Process.*, vol. 54, no. 8, pp. 3166–3179, Aug. 2006.

[7] B. Gaffhey and A. D. Pagan, "Walsh Hadamard transform preceded MB-OFDM: An improved high data rate ultrawideband system," in *Proc. IEEE 17th Int. Symp. Personal, Indoor, Mobile Radio Commun.*, Helsinki, Finland, 2006, p. 5.

[8] C. F. Chan, "Efficient implementation of class of isotropic quadratic filters by using Walsh-Hadamard transform," *Electron. Lett.*, vol. 35, no. 16, pp. 1306–1308, 1999.

[9] W. S. Liao, B. S. Lin, B. S. Lin, H. D. Wu, and F. C. Chong, "Ambient noise canceller in pulmonary sound using WHT transform domain adaptive filter," in *Proc. IEEE 24th Annu. Int. Conf. Eng. Med. Biol. Soc.*, Houston, TX, USA, 2002, vol. 1, pp. 86–87.

[10] R. S. Stankovic, "Some remarks on terminology in spectral techniques for logic design: Walsh transform and Hadamard matrices," *IEEE Trans. Comput.-Aided Design Integr. Circuits Syst.*, vol. 17, no. 11, pp. 1211–1214, Nov. 1998.
[11] L. Zhang, Z. H. Lin, and Z. W. Lv, "Technology mapping and Hadamard transform," in *Proc. IEEE Int. Conf. Commun., Circuits, Syst., West Sino Expo.*, 2002, pp. 1381–1385.
[12] L. Zhihua and Z. Qishan, "Ordering of Walsh functions," *IEEE Trans. Electromagn. Compat.*, vol. EMC-25, no. 2, pp. 115–19, 1983.
[13] S.-M. Phoong and K.-Y. Chang, "Antipodal paraunitary matrices and their application to OFDM systems," *IEEE Trans. Signal Process.*, vol. 53, no. 4, pp. 1374–1386, 2005.
[14] S.-M. Phoong and Y.-P. Lin, "Lapped Hadamard transforms and filter banks," in *Proc. Int. Conf. Acoust., Speech, Signal Process. (ICASSP)*, 2003, vol. 6, pp. VI–509–VI–512.
[15] S. Rahardja and B. J. Falkowski, "Family of unified complex Hadamard transforms," *IEEE Trans. Circuits Syst. II*, vol. 46, no. 8, pp. 1094–1100, 1999.
[16] B. J. Falkowski and S. Rahardja, "Complex Hadamard transforms: Properties, relations and architecture," *IEICE Trans. Fundam. Electron. Commun. Comput. Sci.*, vol. E87-A, no. 8, pp. 2077–2083, 2004.
[17] A. Aung, B. P. Ng, and S. Rahardja, "Sequency-ordered complex Hadamard transform: Properties, computational complexity and applications," *IEEE Trans. Signal Process.*, vol. 56, no. 8, pp. 3562–3571, 2008.
[18] A. Aung, B. P. Ng, and S. Rahardja, "Conjugate symmetric sequency-ordered complex Hadamard transform," *IEEE Trans. Signal Process.*, vol. 57, no. 7, pp. 2582–2593, 2009.
[19] S. Bouguezel, M. O. Ahmad, and M. N. S. Swamy, "An efficient algorithm for the conjugate symmetric sequency-ordered complex Hadamard transform," in *Proc. ISCAS*, 2011, pp. 1516–1519.
[20] J. Wu, L. Wang, G. Yang, L. Senhadji, L. Luo, and H. Shu, "Sliding conjugate symmetric sequency-ordered complex Hadamard transform: fast algorithm and applications," *IEEE Trans. Circuits Syst. I*, vol. 59, no. 6, pp. 1321–1334, 2012.
[21] J. Liang and T. D. Tran, "Fast multiplierless approximations of the DCT with the lifting scheme," *IEEE Trans. Signal Process.*, vol. 49, no. 12, pp. 3032–3044, 2001.
[22] T. D. Tran, "The binDCT: fast multiplierless approximation of the DCT," *IEEE Signal Process. Lett.*, vol. 7, no. 6, pp. 141–144, 2000.
[23] S. Kyochi, Y. Tanaka, and M. Ikehara, "On factorizations of conjugate symmetric Hadamard transform and its relationship with DCT," in *Proc. Int. Conf. Acoust., Speech, Signal Process. (ICASSP)*, 2012, pp. 3477–3480.
[24] W. Sweldens, "The lifting scheme: A custom-design construction of biorthogonal wavelets," *Appl. Comput. Harmon. Anal.*, vol. 3, no. 2, pp. 186–200, 1996.
[25] W. Chen, C. H. Smith, and S. Fralick, "A fast computational algorithm for the discrete cosine transform," *IEEE Trans. Commun.*, vol. COMM-25, no. 9, pp. 1004–1009, 1977.
[26] C. Loeffler, A. Ligtenberg, and G. S. Moschytz, "Practical fast 1-D DCT algorithms with 11 multiplications," in *Proc. Int. Conf. Acoust., Speech, Signal Process. (ICASSP)*, 1989, vol. 2, pp. 988–991.
[27] A. Said and W. A. Pearlman, "A new, fast, and efficient image codec based on set partitioning in hierarchical trees," *IEEE Trans. Circuits Syst. Video Technol.*, vol. 6, no. 3, p. 243,250, Jun. 1996.

Seisuke Kyochi (S'08–M'10) received his B.S. in mathematics from Rikkyo University in Toshima, Japan, in 2005 and his M.E. and Ph.D. from Keio University in Yokohama, Japan, in 2007 and 2010. He has been a researcher at the NTT Cyberspace Laboratories from 2010 to 2012. In 2012, he joined the Faculty of Environmental Engineering at The University of Kitakyushu as a Lecturer. His research areas include the theory and design of wavelets/filter banks for efficient image processing applications.

Yuichi Tanaka (S'02–M'02) received the B.E., M.E. and Ph.D. degrees in electrical engineering from Keio University, Yokohama, Japan, in 2003, 2005 and 2007, respectively. He was a Postdoctoral Scholar at Keio University, Yokohama, Japan, from 2007 to 2008, and supported by the Japan Society for the Promotion of Science (JSPS). From 2006 to 2008, he was also a visiting scholar at the University of California, San Diego (Video Processing Group supervised by Prof. T. Q. Nguyen). From 2008 to 2012, he was an Assistant Professor in the Department of Information Science, Utsunomiya University, Tochigi, Japan. Since 2012, he has been an Associate Professor in Graduate School of BASE, Tokyo University of Agriculture and Technology, Tokyo, Japan. His current research interests are in the field of multidimensional signal processing which includes: signal processing on graphs, image and video processing with computer vision techniques, distributed video coding, objective quality metric, and effective spatial-frequency transform design. He was a recipient of the Yasujiro Niwa Outstanding Paper Award in 2010 and the TELECOM System Technology Award in 2011. Since 2013, he has been an Associate Editor of *IEICE Transactions Fundamentals*.